ChemBioChem

Research Article
doi.org/10.1002/cbic.202200632

Chemistry Europe
European Chemical Societies Publishing

www.chembiochem.org

Bacterial Dehydrogenases Facilitate Oxidative Inactivation and Bioremediation of Chloramphenicol

Lei Zhang,[a] Marina Toplak,[a] Raspudin Saleem-Batcha,[b] Lars Höing,[e] Roman Jakob,[c] Nico Jehmlich,[d] Martin von Bergen,[d] Timm Maier,[c] and Robin Teufel*[e]

Antimicrobial resistance represents a major threat to human health and knowledge of the underlying mechanisms is therefore vital. Here, we report the discovery and characterization of oxidoreductases that inactivate the broad-spectrum antibiotic chloramphenicol via dual oxidation of the C3-hydroxyl group. Accordingly, chloramphenicol oxidation either depends on standalone glucose-methanol-choline (GMC)-type flavoenzymes, or on additional aldehyde dehydrogenases that boost overall turnover. These enzymes also enable the inactivation of the chloramphenicol analogues thiamphenicol and azidamfenicol, but not of the C3-fluorinated florfenicol. Notably, distinct isofunctional enzymes can be found in Gram-positive (e.g., *Streptomyces* sp.) and Gram-negative (e.g., *Sphingobium* sp.) bacteria, which presumably evolved their selectivity for chloramphenicol independently based on phylogenetic analyses. Mechanistic and structural studies provide further insights into the catalytic mechanisms of these biotechnologically interesting enzymes, which, in sum, are both a curse and a blessing by contributing to the spread of antibiotic resistance as well as to the bioremediation of chloramphenicol.

Introduction

The resistance of microbial pathogens against clinically used antibiotics represents an exacerbating threat to the medical treatment of infectious diseases and worldwide health care systems. A recent study estimates ca. 1.27 million and 4.95 million deaths in 2019 attributed to and associated with bacterial antimicrobial resistance (AMR), respectively, which may thus surpass other major diseases such as HIV infection and malaria.[1] It is therefore crucial to gain a fundamental understanding of the spread and underlying mechanisms of AMR to develop counterstrategies and to ensure the future efficacy of antibiotic treatment. One of the earliest antibiotics in clinical use was chloramphenicol (CAP), originally isolated from *Streptomyces venezuelae* in 1947. CAP inhibits both Gram-positive and Gram-negative bacteria and was the first antibiotic to be synthetically produced in large scale.[2] CAP features a *p*-nitrophenyl group attached to the C1 of a 1,3-propanediol backbone as well as an *N*-dichloroacetyl substituent at C2 with two chiral centers (C1 and C2) (Figure 1). Bacterial CAP biosynthesis depends on a nonribosomal peptide synthetase and starts from *p*-amino-L-phenylalanine and dichloroacetyl precursors.[3] Of the four possible diastereomers, only the naturally produced D-*threo* compound possesses antibiotic activity and generally only a few minor alterations particularly at the C-3 hydroxyl and the nitro groups of the CAP pharmacophore are tolerated that do not result in the loss of activity.[2b] Still, this limited modifiability has been exploited in human and veterinary medicine for the generation of (semi)synthetic derivatives, which helped to alleviate some rare but severe side effects, most notably fatal aplastic anemia, bone marrow suppression and gray baby syndrome. These analogues comprise thiamphenicol (sulfomethyl substitution of the nitro group), florfenicol (like thiamphenicol but with additional fluoro substitution of the C3-hydroxyl) and azidamfenicol (dichloromethyl group replaced by a methyl azide) (Figure 1C).[2b,4]

In principle, the stable amphiphilic CAP is unionized under physiological conditions and therefore able to traverse cellular membranes,[2b] although porins are often required in the outer membrane of Gram-negative bacteria, as exemplified by *Salmonella* Typhi.[5] Once within the cell, bacteriostatic CAP and its derivatives shut down protein biosynthesis through binding to the peptidyltransferase of the 50S subunit of the bacterial ribosome.[6] However, bacteria may counteract the inhibitory

[a] *L. Zhang, Dr. M. Toplak*
Faculty of Biology, University of Freiburg
Schänzlestrasse 1, 79104 Freiburg (Germany)
[b] *R. Saleem-Batcha*
Institute of Pharmaceutical Sciences
University of Freiburg, Albertstrasse 25, 79104 Freiburg (Germany)
[c] *Dr. R. Jakob, Prof. T. Maier*
Biozentrum, University of Basel
Spitalstrasse 41, 4056 Basel (Switzerland)
[d] *Dr. N. Jehmlich, Prof. Dr. M. von Bergen*
Department of Molecular Systems Biology
Helmholtz-Centre for Environmental Research
UFZ GmbH, Leipzig (Germany)
and
German Centre for Integrative Biodiversity Research
(iDiv) Halle-Jena-Leipzig
Puschstraße 4, 04103 Leipzig, Germany
and
University of Leipzig, Faculty of Life Sciences, Institute of Biochemistry
Brüderstraße 34, 04103 Leipzig, Germany
[e] *L. Höing, Prof. R. Teufel*
Pharmaceutical Biology
Department of Pharmaceutical Sciences
University of Basel, Klingelbergstrasse 50, 4056 Basel (Switzerland)
E-mail: robin.teufel@unibas.ch
Homepage: https://pharma.unibas.ch/de/research/research-groups/pharmaceutical-biology-2241

Supporting information for this article is available on the WWW under https://doi.org/10.1002/cbic.202200632

This article is part of the Special Collection ChemBioTalents2022. Please see our homepage for more articles in the collection.

effects of CAP, e.g., by target (=ribosome) mutation, permeability barriers, or (multi) drug exporters.[4a,7] Additionally, enzymatic resistance is typically mediated by 3-*O*-acetyltransferases that modify the C3-hydroxyl group of CAP, which thereby loses its affinity for the ribosome.[8] Furthermore, natural producer strains protect themselves with 3-*O*-phosphotransferases or via an amide-bond cleaving hydrolase (Figure 1A).[2b,9] Notably, these enzyme activities have also been reported in bacteria that do not produce CAP.[2b,4a] Finally, flavin-dependent nitroreductases were identified that fully reduce the nitro group of CAP to the corresponding amine (Figure 1A).[10] Here, we report the serendipitous discovery of a prevalent strategy for the permanent enzymatic inactivation of antibiotic CAP in bacteria, which foremost relies on flavin adenine dinucleotide (FAD)-dependent enzymes of the glucose-methanol-choline (GMC) oxidoreductase superfamily.[11] These enzymes primarily function as C3-alcohol dehydrogenases (referred to as CAP-ADHs+ and CAP-ADHs- for Gram-positive and Gram-negative bacteria, respectively) that can furthermore over-oxidize the aldehyde intermediate to the corresponding carboxylic acid. Alternatively, dedicated aldehyde dehydrogenases (CAP-ALDHs) may mediate the second oxidation step to drive production of the inactive "carboxy-CAP" (Figure 1B).

Results and Discussion

Nocardiopsis sp. inactivate chloramphenicol by dual oxidation of the C3-hydroxy group

In search of urgently needed new antibiotics, chemical elicitors are commonly added to bacterial cultures in order to trigger secondary metabolite production. In this context, the Gram-positive, spore-forming *Nocardiopsis synnemataformans* DSM 44143, whose biosynthetic potential remains unexplored similar to many other *Nocardiopsis* spp.,[12] was cultured in our laboratory.[13] However, when exposing *N. synnemataformans* to sublethal concentrations of CAP in an attempt to elicit secondary metabolism, high-performance liquid chromatography (HPLC) analysis rather indicated the chemical modification of CAP (Figure 2A). The formed derivative featured a virtually identical UV-Vis spectrum to CAP and was therefore initially suspected to result from canonical *N*-acetylation (Figure S1AB).

Robin Teufel received his Diploma in Biology from the University of Freiburg in 2008, where he also completed his PhD studies (2011). He then conducted his postdoctoral training at the Scripps Institution of Oceanography (2012–2014), after which he returned to Freiburg as a research group leader (2015–2021). In 2022, he joined the Department of Pharmaceutical Sciences, University of Basel as Associate Professor of Pharmaceutical Biology. His research interests are focused on natural products, biosynthesis and enzymology.

Yet, liquid chromatography high resolution mass spectrometry (LC-HRMS) analysis surprisingly revealed a mass difference of +13.978 Da (336.999 $[M+H]^+$) compared to CAP (323.021 $[M+H]^+$), indicating the loss of two hydrogens and the addition of one oxygen atom (Figure S1CD). Accordingly, this suggested that the primary alcohol at the C3 position had been enzymatically converted to the corresponding carboxylic acid. Indeed, upscaling of the *N. synnemataformans* cultures (supplemented with CAP) and subsequent purification of the derivative followed by NMR analysis (^1H, ^{13}C, COSY, HSQC, HMBC, Figure S2–6 & Table S1) confirmed the C3 oxidation and the formation of carboxy-CAP (Figure 1). Next, the antimicrobial activity of carboxy-CAP was assessed by agar diffusion tests and compared with the native antibiotic. Evidently, carboxy-CAP lost its antibiotic activity both against Gram-positive and Gram-negative bacteria (Figure S7 and Table S2), indicating that this enzymatic transformation is a means of CAP inactivation. Further degradation of carboxy-CAP by *N. synnemataformans* could not be observed (Figure 2A).

CAP oxidation mediates increased basal resistance and may rely on flavoprotein dehydrogenases

At the time of this finding, CAP inactivation by oxidation of the C3-hydroxy group had not been reported to the best of our knowledge, prompting us to further investigate this phenomenon. First, the rates of CAP inactivation were determined in the cell-free lysates of *N. synnemataformans* cultures that were sacrificed at different growth stages. In all cases, low basal activity for CAP oxidation was observed with ca. 0.03 ± 0.01 nmol min^{-1} mg^{-1} protein, allowing the bacteria to grow up to a concentration of 30 μg ml^{-1} CAP in solution (typical MICs for Gram-positive bacteria range between 2.5 and 20 μg ml^{-1}, Table S3). Notably, the addition of sublethal concentrations of CAP (12 μg ml^{-1}) to the growing cultures had no pronounced effect on the specific activity for CAP inactivation in the cell-free lysate (Figure 2D), suggesting that the involved enzyme(s) are constitutively produced rather than induced upon exposure to CAP. When considering the enzyme(s) involved in catalyzing the envisaged two-step oxidation, various types and combinations thereof are conceivable, including iron-dependent cytochrome P450s (CYPs), copper-dependent alcohol oxidases, separate flavin- and/or $NAD(P)^+$-dependent alcohol and aldehyde dehydrogenases/oxidases, or standalone flavin-dependent choline oxidase like enzymes.[14] To obtain more information, ^{18}O-isotope labelling experiments coupled to HR-LCMS analysis were conducted, which clearly showed ^{18}O incorporation from water ($H_2{}^{18}O$) rather than from molecular oxygen ($^{18}O_2$), thus ruling out the involvement of oxygenases in this transformation (Figure S8A-C). Notably, up to two ^{18}O derived from $H_2{}^{18}O$ were observed in carboxy-CAP (Figure S8C), which pointed toward the formation of an aldehyde intermediate that spontaneously exchanges with water via a transiently stabilized gem-diol,[15] before the second ^{18}O is incorporated upon formation of the carboxyl group. Next, different additives and conditions were tested to further probe the enzymatic reactions. While the

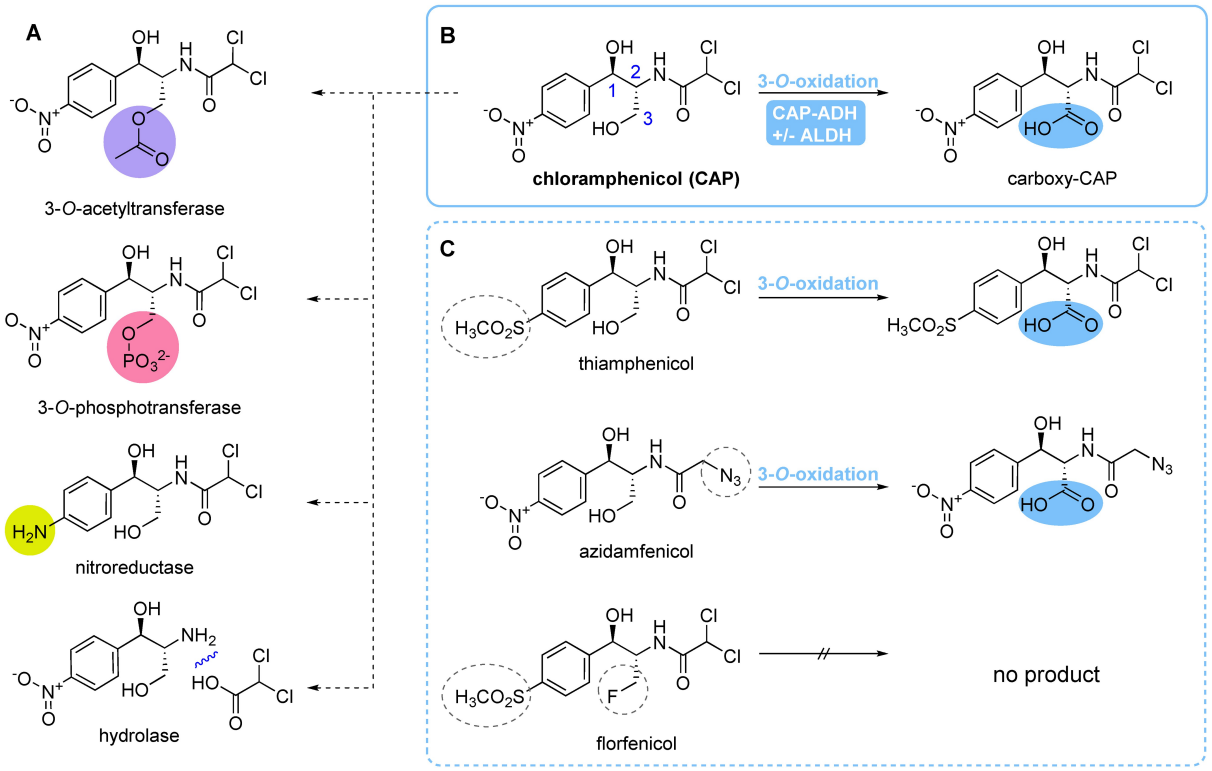

Figure 1. Enzymatic inactivation mechanisms for chloramphenicol and its (semi)synthetic derivatives. A) Known enzymatic CAP inactivation mechanisms. B) CAP inactivation by 3-*O*-dual oxidation reported herein, which is mediated by dedicated GMC oxidoreductases (CAP-ADHs) and (optional) aldehyde dehydrogenases (ALDHs). C) (Semi)synthetic CAP derivatives (modified structural features are highlighted by dashed outlines) can also be oxidatively inactivated with the exception of florfenicol. Note that other forms of CAP resistance, e.g. via drug exporters, are not shown.

presence of $NADP^+/NAD^+$ hardly affected CAP-turnover, the addition of the artificial oxidant 2,6-dichlorophenolindophenol (DCIP) resulted in a drastic ca. seven-fold rate increase of carboxy-CAP formation (Figure 2B, Figure S10A). Under anoxic conditions, the conversion of CAP was completely dependent on DCIP (Figure S10B), suggesting that the initially observed enzyme activity under aerobic conditions is due to low O_2 reactivity. Overall, these results suggested the involvement of a flavoprotein dehydrogenase, which (in contrast to a flavoprotein oxidase) only sluggishly reacts with O_2 following substrate turnover and therefore innately relies on other dedicated electron acceptors (e.g., electron transferring flavoproteins (ETFs), quinones, or cytochromes) for restoration of the oxidized flavin adenine dinucleotide cofactor (FAD_{ox}) from FAD_{red}.[11b,14b,16]

Whole cell proteomics and native protein purification reveal a novel GMC-like flavoprotein dehydrogenase for CAP inactivation

To unambiguously identify the involved enzymes, first, a whole cell proteomics approach was attempted, in which *N. synnemataformans* cells were compared at different growth stages with low and high specific activity for CAP oxidation. This proved challenging, as a distinct regulation pattern could not be discerned (Figure 2D). Nonetheless, the proteomes of two cultures with low specific activities (0.004 and 0.005 nmol min^{-1} mg^{-1}, respectively) as control and two additional cultures with high specific activities (0.036 and 0.039 nmol min^{-1} mg^{-1}, respectively) could eventually be compared. The search for upregulated enzyme candidates was particularly focused on members of the flavin-dependent glucose-methanol-choline (GMC)- and vanillyl-alcohol oxidase (VAO)-type families that often oxidize primary alcohols,[11b,14b,17] while not ruling out other types of oxidoreductases. However, a clear candidate for which the degree of upregulation correlated with the measured specific activities was not apparent. These results may indicate unstable enzyme(s) and/or very low amounts of the corresponding peptide fragments possibly below the detection limit, consistent with the overall low enzyme activity measured in the cell-free lysates. Therefore, the purification of the native enzyme(s) from the cell free lysates was attempted via column chromatography by assessing the rate of CAP oxidation in the respective fractions by HPLC. Despite challenges resulting from the low abundance and limited stability of the enzyme(s), a substantial enrichment of the CAP oxidation activity could be achieved over three chromatographic steps using anion exchange, hydrophobic interaction and size exclusion columns (Figure S11A–C and Table S4). Moreover, the active fractions retained their proficiency to fully oxidize CAP, suggesting that a single enzyme or, alternatively, a stable complex of enzymes is responsible for the two-step oxidation. When the active

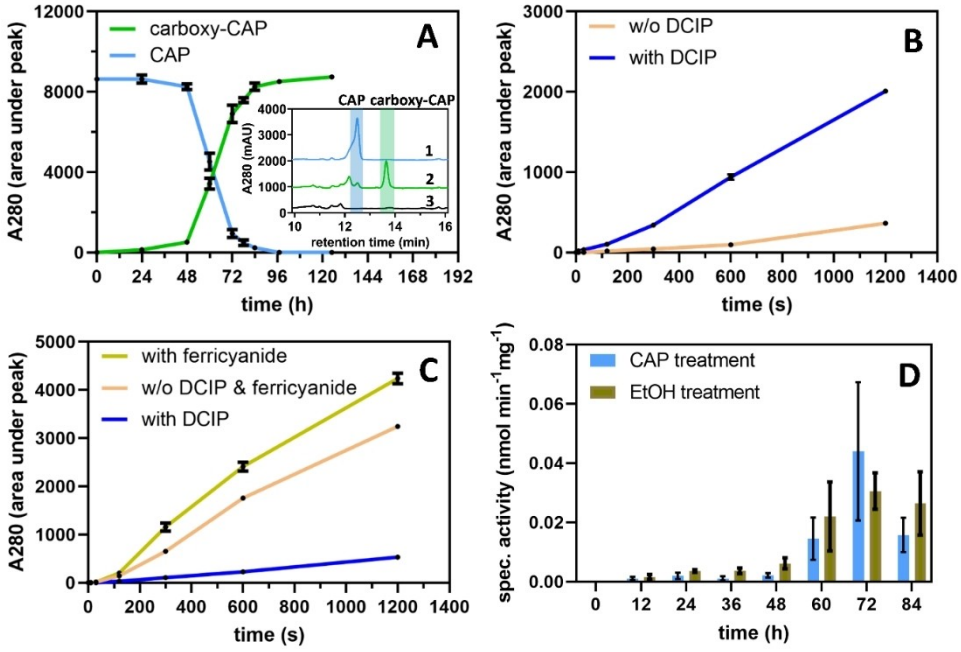

Figure 2. Enzymatic carboxy-CAP formation. A) Carboxy-CAP formation and CAP consumption over time in *N. synnemataformans* cultures supplemented with sublethal concentrations of CAP (y-axis shows increase/decrease of peak areas based on A280 nm). The small inset shows HPLC-DAD traces of: 1) Extract of GYM-NaCl medium supplemented with CAP; 2) Extract of *N. synnemataformans* culture supplemented with CAP (dissolved in EtOH); 3) Extract of *N. synnemataformans* culture treated with EtOH. B) Carboxy-CAP formed from CAP in aerobic CAP-ADH+^{NR} assays in the presence or absence of DCIP. C) Carboxy-CAP produced in the aerobic CAP-ADH-^{NB} assays in the presence or absence of DCIP / potassium ferricyanide. D) Specific activities for CAP-oxidation in *N. synnemataformans* cell free lysates of cultures treated with either CAP (dissolved in EtOH; in blue) or EtOH only (control; in brown), respectively. Error bars indicate the SEM (n = 3).

fractions of the final column were analyzed by sodium dodecyl sulfate-polyacrylamide gel electrophoresis (SDS-PAGE), only one prominent protein band remained in the range of 45–65 kDa, in which the enzyme candidates were expected. Subsequent excision and proteolytic digestion of the band followed by HR-LCMS analysis revealed fragments of only a few proteins, one of which, gratifyingly, represented a putative GMC-like flavoprotein (NCBI-accession number, WP_017563851.1) (Figure S11D and Table S5). Upon revisiting the proteomics data, fragments of this protein could indeed be identified at very low abundance that were absent in the control samples, further supporting that this enzyme represents the sought-after CAP-inactivating enzyme (Table S6–7).

Flavoprotein dehydrogenases are employed for CAP resistance as well as catabolism in Gram-positive and Gram-negative bacteria

To confirm the CAP-oxidizing activity and characterize the identified enzyme, heterologous protein production was attempted (Table S8). However, despite numerous tested expression vectors, producer strains (including *E. coli* strain BL21 Codon Plus RP pL1SL2 producing *Streptomyces coelicolor* chaperonins GroEL1, GroEL2 and GroES) and protein tags,[18] the enzyme proved to be largely insoluble. Nonetheless, the obtained amounts of protein were sufficient for *in vitro* assays, allowing to verify that carboxy-CAP formation is indeed mediated by this single flavin-dependent CAP dehydrogenase from *N. synnemataformans* (CAP-ADH+^{NS}) (Figure S12A). This is consistent with previous reports of rare GMC-like oxidases that are capable of over-oxidizing their substrates and further convert the aldehyde intermediates to the respective carboxylic acids, as exemplified by choline oxidase and 5-hydroxymethylfurfural oxidase.[11b,14b,c,19]

Interestingly, in the course of the identification and characterization of CAP-ADH+^{NS}, two groups reported novel catabolic pathways for CAP in the Gram-negative α-Proteobacteria *Sphingobium* sp. CAP-1 and for CAP/thiamphenicol in *Sphingomonas* sp. CL5.1 that were isolated from activated sludge samples.[20] Remarkably, carboxy-CAP also proved to be a key intermediate that is likely further broken down via *p*-nitrosobenzoate, protocatechuate and ring-opened intermediates, ultimately yielding central metabolites.[20a] While the responsible enzymes for CAP oxidation were not clearly identified, comparative proteome analyses showed the upregulation of putative oxidoreductases,[20a,c] These upregulated enzymes resembled GMC-type alcohol dehydrogenases (both *Sphingobium* sp. CAP-1 and *Sphingomonas* sp. CL5.1) and NAD(P)$^+$-dependent aldehyde dehydrogenases (only *Sphingobium* sp. CAP-1), whose genes were co-localized in the *Sphingobium* sp. CAP-1 genome (Figure 3B) indeed making them prime candidates for effectuating an analogous CAP oxidation.[20a] To further investigate this, the genes from

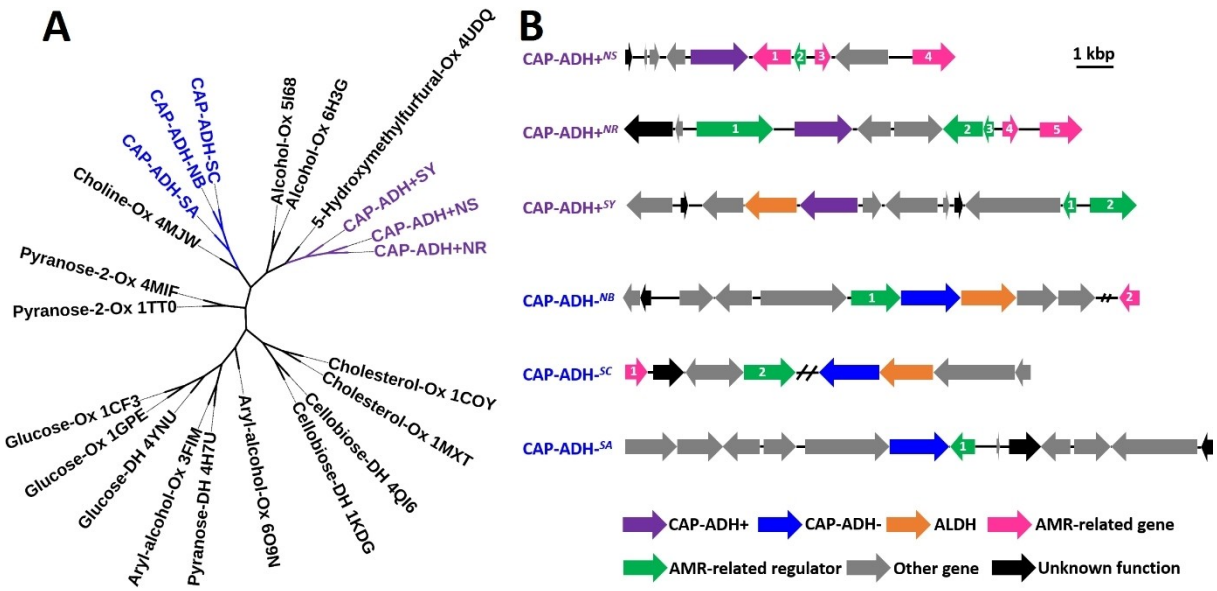

Figure 3. Evolutionary relationships among GMC family flavoproteins and gene environments of *cap-adh* genes. A) Phylogenetic distance tree of GMC family flavoenzymes including CAP-inactivating enzymes from Gram-positives (CAP-ADHs+; in purple) and Gram-negatives (CAP-ADHs-; in blue). B) Graphical representation of the gene environments of the *cap-adh* genes from *Nocardiopsis synnemataformans* DSM 44143 (encodes CAP-ADH+^{NS}), *Nocardiopsis* sp. RV163 (CAP-ADH+^{NR}), *Streptomyces* sp. YIM 130001 (CAP-ADH+^{SY}), *Novosphingobium* sp. B 225 (CAP-ADH-^{NB}), *Sphingobium* sp. CAP-1 (CAP-ADH-^{SC}) and *Steroidobacter agaridevorans* SA29-B (CAP-ADH-^{SA}). The predicted functions of the AMR-related proteins encoded by the numbered genes (shown in red and green) are listed in Table S9 for each bacterium, including accession and contig numbers.

Sphingobium sp. CAP-1 were cloned and the encoded enzymes, which presumably function as C3-oxidizing CAP alcohol dehydrogenase (CAP-ADH-^{SC}) and aldehyde dehydrogenase (CAP-ALDH^{SC}), respectively, were heterologously produced (Figure S13-16). Due to higher yields and increased protein stability, these enzymes could be purified without difficulty and characterized in more detail. Accordingly, the enzymatic oxidation of CAP into carboxy-CAP was first confirmed by *in vitro* assays with CAP-ADH-^{SC} (Figure S12B) and/or CAP-ALDH^{SC}, which furthermore showed that the addition of CAP-ALDH^{SC} significantly boosted overall turnover (Figure S17), while this enzyme alone could not convert CAP (Figure S18A). Interestingly, the increase in carboxy-CAP formation was also observed for CAP-ADH+^{NS} when CAP-ALDH^{SC} was added to the assays (Figure S19). Overall, these experiments support the idea that CAP-ADH-^{SC} and CAP-ALDH^{SC} represent dedicated enzymes for CAP oxidation in *Sphingobium* sp. CAP-1.

Enzyme characterization and phylogenetic analysis reveal the widespread occurrence of CAP oxidizing and inactivating oxidoreductases

To gain a better understanding of the prevalence of the CAP inactivating enzymes, BLAST searches and phylogenetic analyses were conducted. First, the surroundings of the genes encoding CAP-ADH+^{NS} and CAP-ADH-^{SC}/ CAP-ALDH^{SC} were inspected, revealing other genes encoding putative AMR-related proteins, fully consistent with the enzymes' proposed role (Table S9). BLASTP searches with CAP-ADH+^{NS} subsequently enabled the identification of numerous other closely related enzyme candidates in Gram-positive bacteria, e.g., from other *Nocardiopsis* spp., *Streptomyces* spp. or *Actinomadura* spp. (Table S10). To further verify their roles and obtain a suitable stable candidate for in-depth mechanistic studies, several homologues of CAP-ADH+^{NS} were heterologously produced (Table S8). Enzymatic assays with CAP-ADH+^{NR} (from *Nocardiopsis* sp. RV163) and CAP-ADH+^{SY} (*Streptomyces* sp. YIM) confirmed that the novel CAP resistance strategy is more prevalent in Gram-positives (Figure S12A and Figure S20). However, similar to CAP-ADH+^{NS}, the enzymes were poorly soluble with His and/or GB1 tags and rendered inactive by MBP tags, which impeded further enzyme characterization despite extensive efforts (Figure S21). Further BLASTP searches revealed homologues of CAP-ADH-^{SC} in numerous Gram-negative bacteria and selected genes were cloned and the corresponding enzymes heterologously produced and characterized (Table S11). Among those, CAP-ADH-^{NB} (*Novosphingobium* sp. B 225; α-Proteobacterium), CAP-ADH-^{SA} (*Steroidobacter agaridevorans*; γ-Proteobacterium), and (*Rhodopseudomonas palustris*; α-Proteobacterium) were tested. Apart from the latter enzyme, which proved to be completely insoluble, all tested enzymes indeed exhibited CAP oxidation activity (Figure S12B and Figures S22–23). Notably, genes encoding ALDHs were found to be co-localized only in some Gram-positive and Gram-negative strains (Figure 3B).

More detailed enzyme characterization showed that the investigated enzymes not only mediate the oxidative inactivation of CAP, but also of the clinically used analogues thiamphenicol and azidamfenicol. In contrast, however, florfeni-

col, whose C3-hydroxy group is substituted with a fluoro group, was expectedly not modified and thus retained its antibiotic activity (Figures S24–25). The addition of DCIP significantly increased substrate turnover for the six tested enzymes with the exception of CAP-ADH-^{NB}. This enzyme proved to be surprisingly reactive toward O_2 and the addition of alternative electron acceptors such as DCIP or potassium ferricyanide did not noticeably boost activity; in contrast, DCIP even inhibited carboxy-CAP formation (Figure 2C). Overall, these data suggest that the GMC-type enzymes mostly function as dehydrogenases rather than oxidases. For members of GMC-like enzymes from Gram-positive and Gram-negative bacteria (CAP-ADH-^{SC}, CAP-ADH-^{NB} and CAP-ADH + ^{NR}), the specific kinetic parameters (K_{Mapp}, k_{catapp}, catalytic efficiency) and pH/temperature optima were determined by spectrophotometric and HPLC-based assays (Figure S26–27 and Table S12). A summary of all protein specifics alongside with other information is given in Table S13–14. Moreover, based on HR-LCMS analysis, the proposed aldehyde intermediate accumulated in the absence of an ALDH (Figure S28). Consistent with that, ^{18}O-labelling assays with $H_2{}^{18}O$ showed that while two ^{18}O atoms were incorporated into carboxy-CAP in assays containing only a GMC-type dehydrogenase, only one ^{18}O was introduced in presence of a dedicated ALDH, corroborating that these enzymes prevent the accumulation of CAP-aldehyde and thus the spontaneous oxygen exchange of the aldehyde with water (Figure S8D–I).

Next, a phylogenetic analysis was conducted and the resulting tree revealed that the GMC-type dehydrogenases of Gram-negatives and Gram-positives clustered separately and were only distantly related, suggesting the independent recruitment and evolvement of these enzymes (Figure 3A and Table S15). However, both enzyme types from Gram-positives and Gram-negatives were most closely related to enzymes capable of over-oxidizing alcohols to the corresponding carboxylic acids. Intriguingly, though, the Gram-positive CAP-inactivating enzymes clustered with 5-hydroxymethylfurfural oxidase from the Gram-negative β-Proteobacterium *Methylovorus* sp. strain MP688, whereas the Gram-negative specimen are more closely related to the GMC oxidase of the Gram-positive *Arthrobacter globiformis* strain ATCC 8010, possibly implying horizontal gene transfer events (Figure 3 and Table S15). Notably, most genes of the (predicted) GMC-type dehydrogenases of Gram-negative and Gram-positive strains featured adjacent or close-by genes for ALDHs to accelerate the second oxidation step and provide a more efficient means of CAP inactivation (Table S11).

CAP-ADH-^{NB} crystal structure and site-directed mutagenesis identify the catalytically important His471

To gain further insights into the mechanism underlying oxidative CAP inactivation, crystallization was attempted with CAP-ADH-^{NB}, which was the most promising candidate according to *in silico* predictions using XtalPred-RF as well as based on yield and stability of the enzyme (Figure S29–31).[21] In vapor-diffusion set-ups, yellow plate-like crystals of CAP-ADH-^{NB} were obtained that diffracted up to 2.1 Å. The protein structure was solved by molecular replacement using an AlphaFold model as template,[22] and showed a GMC-like architecture with an N-terminal FAD binding domain (GMC_oxred_N (Pfam00732)) and a C-terminal substrate binding domain (Figure 4A).[11b,23] Of the 540 CAP-ADH-^{NB} protein residues, 458 residues could be modeled, but several loop regions were not resolved in the electron density map including loops likely involved in substrate binding (Figure 4B). Not surprisingly, given these dynamic loops surrounding the active site, co-crystallization and soaking experiments with CAP or florfenicol did not result in additional electron density within the active site despite our best efforts. The structurally closest CAP-ADH-^{NB} homologue is choline oxidase with a backbone r.m.s.d. of 1.6 Å and main differences in the less conserved C-terminal substrate binding

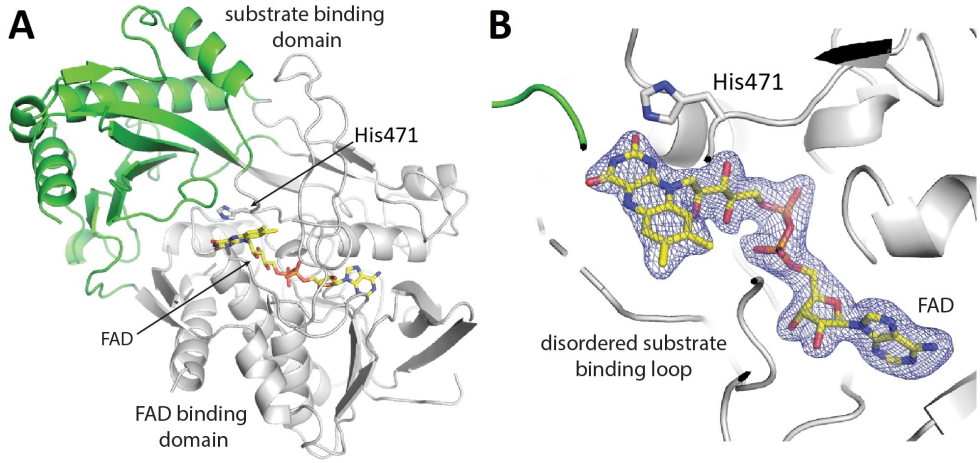

Figure 4. Overall structure of CAP-ADH-^{NB} and close-up view of the FAD. (A) Structure of CAP-ADH-^{NB}. The FAD-binding domain is shown in grey, the substrate binding domain in green. The FAD (yellow) and the His471 are shown as sticks. (B) Close-up on the FAD (stick representation) with a Polder OMIT mF_{obs}-DF_{model} electron density map contoured at 3σ (slate color).[26] The catalytically important His471 side chain and the location of the disordered substrate binding loop residues are indicated.

domain.[11b,19a,b,24,25] Like the majority of GMC-type enzymes, CAP-ADH-^{NB} features a non-covalently, but tightly bound FAD cofactor (Figure 4B).[11b,14b] A highly conserved active-site histidine typically acts as catalytic base to promote substrate oxidation.[11b,24] In CAP-ADH-^{NB}, His471 is found in that position, which therefore likely activates the substrate by deprotonating the C3-hydroxy group. To confirm the role of His471, site-directed mutagenesis was conducted and the CAP-ADH-^{NB}-H471 A variant biochemically analyzed. As expected, the enzyme variant was completely inactive and no longer capable of oxidizing CAP. Similar to this, the enzymes from the Gram-positive bacteria such as CAP-ADH+^{NS} also feature a conserved histidine that most likely adopts the same function.

Based on these data, the mechanism of the GMC-type flavoprotein dehydrogenases reported herein most likely involves the deprotonation of the C3-alcohol by the conserved histidine residue, followed by a direct hydride transfer from C3 to N5 of FAD_{ox}, as previously reported for other enzyme family members. Subsequent to alcohol oxidation, the FAD_{red} cofactor has to be reoxidized, for which most CAP-ADHs presumably depend on dedicated intracellular electron acceptors rather than on O_2. Then, following spontaneous aldehyde hydration, a second oxidation cycle can be initiated via deprotonation of one of the C3-hydroxyl groups and subsequent hydride transfer, ultimately affording carboxy-CAP. Alternatively, NAD(P)$^+$-dependent ALDHs such as CAP-ALDH^{NB} may be employed for this step, which instead rely on a catalytic cysteine (C295 for CAP-ALDH^{NB}) for the initial attack on the carbonyl. After the hydride transfer from the resulting tetrahedral intermediate to NAD(P)$^+$, water is activated by a catalytic glutamate (E249) to attack the transient thioester and to expel the cysteine thiol under formation of the carboxyl group (Figure 5). More biochemical and structural experiments will be required to get further insights into the underlying reaction mechanisms.

Conclusion

To counteract rapidly spreading AMR, a multifaceted approach is required that necessitates a comprehensive understanding of bacterial strategies to evade clinically used antibiotics. In this work, enzymatic CAP oxidation is showcased and scrutinized as key to both antibiotic inactivation as well as bioremediation. This dual oxidation relies on either standalone GMC-type flavoprotein dehydrogenases or additionally on NAD(P)$^+$-dependent ALDHs for the second step. While flavoenzymes more commonly participate in the biosynthesis of natural products,[16b,27] there is also precedence for their role in degradation and inactivation of toxic metabolites, e.g., by RIFMO that inactivates the antibiotic rifampicin via *N*-hydroxylation.[28] Presumably, flavoenzymes proved advantageous for the first step in CAP inactivation due to their tunable and typically higher redox potentials compared to NAD(P)$^+$-dependent dehydrogenases, for which the thermodynamic equilibrium disfavors alcohol oxidation.[29] GMC-type enzymes most often catalyze the oxidation of primary and secondary alcohols and in rare cases also the over-oxidation to the corresponding carboxylic acid. Hence, it is likely no coincidence that at least two different GMC-type enzymes have been selected in the course of bacterial evolution to effectuate the oxidative inactivation of CAP (see Figure S32 for sequence alignments). Due to their typical high stability, such GMC oxidoreductases would also be prime candidates for biotechnological applications.

For the Gram-negative type, as exemplified by CAP-ADH-^{NB}, the presented enzyme structure and mutagenesis studies confirmed a critical catalytic base for substrate activation. In addition to CAP, the reported enzymes are also capable of inactivating thiamphenicol and azidamfenicol but not florfenicol analogous to the prevalent acetyltransferases.[8] It is interesting to see that some but not all bacteria recruited NAD(P)$^+$-dependent ALDHs in addition to the GMC-type enzymes. Thereby, the overall turnover is improved and the accumulation of toxic aldehydes, which are prone to react with

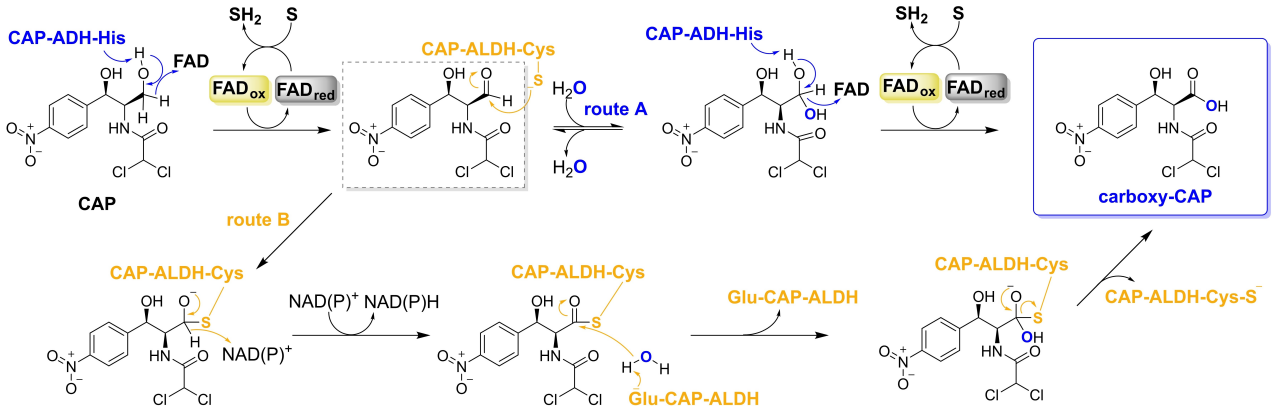

Figure 5. Proposed catalytic mechanism of CAP-inactivating oxidoreductases. The first oxidation of the C3-hydroxy group is catalyzed by GMC oxidoreductases and most likely involves a catalytic histidine side chain that acts as base to initiate oxidation. A hydride is then transferred to the FAD cofactor, which has to be reoxidized with the help of O_2 or another dedicated substrate S. The aldehyde intermediate can then be processed again by these enzymes (route A, blue) or, alternatively, by separate ALDHs (route B, orange).

macromolecules such as proteins or DNA, can be minimized. Evidently, standalone GMC-type enzymes cannot fully prevent the accumulation of the aldehyde intermediate, presumably because the enzymes have to release the aldehyde intermediate before FAD_{red} can be reoxidized by the respective electron acceptor, which may represent the rate-limiting step(s) overall. As a result, CAP and the produced aldehyde intermediate would then also compete for the same active site. It is noteworthy that the native electron acceptor for these enzymes may be a compound or protein similar to some other GMC oxidoreductases (e.g., glucose dehydrogenase and cellobiose dehydrogenase) and the assays conducted with DCIP as artificial electron acceptor may therefore not fully reflect the *in vivo* state.[14b] In contrast to these GMC-enzymes, the $NAD(P)^+$-dependent ALDHs are optimized for aldehyde oxidation and rely on catalytic cysteine and glutamate residues. It is quite possible that protein-protein interactions between the GMC oxidoreductases and the ALDHs may help to prevent the accumulation of toxic aldehydes, e.g., by substrate channeling.

The reported oxidative inactivation of CAP allows bacteria to efficiently dispose or even make use of this lethal toxin. First, the reaction provides two reduction equivalents to the bacteria, which can be utilized to generate ATP under aerobic conditions. This is in contrast to the most common strategies, *O*-acetylation or phosphorylation,[8,30,31] that rather consume energy-rich acetyl-CoA or ATP. Second, the inactivation is more robust, as carboxylates are typically only reduced by rare substrate specific ATP- and NADPH-dependent carboxylic acid reductases,[32] whereas deacetylation or dephosphorylation are common enzymatic reactions. Third, in case of CAP catabolizing bacteria, the negatively charged carboxy-CAP is unlikely to traverse the membrane and escape the cell, which facilitates its full degradation. In addition to reduced membrane permeability, the loss of antibiotic activity is likely ensured by decreased affinity for the 50S subunit of the ribosome, as the newly introduced negative charge of the carboxylate would be in direct clashing distance to the phosphate backbone of the ribosomal RNA moiety, thus leading to electrostatic repulsion (Figure S33).[6b]

Taken together, our study reports a widespread strategy for oxidative CAP detoxification in phylogenetically diverse bacteria. The discovered mechanism is on the one hand instrumental to the bioremediation of broad-spectrum antibiotics and thus likely reduces the selection pressure and the spread of resistance in the environment, but on the other hand actively contributes to resistance against CAP and its clinically used derivatives. It is surprising that many decades after the discovery of CAP inactivating acetyltransferases and phosphotransferases, distinct widespread enzyme types and principles for CAP inactivation can still be unearthed. It will be interesting to see whether other GMC-type enzymes or possibly even completely unrelated enzymes (e.g., other flavoenzymes or CYPs) that catalyze analogous oxidations of the C3-hydroxy group of CAP and derivatives thereof will be discovered in the future.

Experimental Section

Bacterial strains: *Nocardiopsis synnemataformans* DSM 44143 (DMSZ), *Bacillus subtilis* subsp. subtilis 168, *Micrococcus luteus* DSM 20030, *Escherichia coli* K12 DSM 498, *Pseudomonas fluorescens* DSM 90090, *Saccharomyces cerevisiae* DSM 1334.

Media: GYM-NaCl medium: 4 g/L glucose, 4 g/L $CaCO_3$, 4 g/L yeast extract, 4 g/L NaCl, and 4 g/L malt extract. LB medium: tryptone 10 g/L, yeast extract 5 g/L and NaCl 10 g/L. DMSZ medium 65: 4 g/L yeast extract, 10 g/L malt extract, 4 g/L D-glucose and 12 g/L agar. DMSZ medium 1: 5 g/L peptone, 3 g/L meat extract and 15 g/L agar, adjust pH to 7.0.

Purification of carboxy-CAP: *N. synnemataformans* was inoculated into twenty 1 L-flasks with 250 mL of GYM-NaCl medium and cultures were incubated at 28 °C, 160 rpm. After 4 days, CAP was added to each culture to a final concentration of 12 μg/mL. After 5 days, the supernatant was harvested by centrifugation (4000 g for 15 min) and extracted two times with an equal volume of EtAOc/MeOH [9:1 (*v*/*v*)] + 1% AcOH. The organic phase was dried over $(NH_4)_2SO_4$ and subsequently was concentrated to dryness using a rotary evaporator. Then the residue was redissolved in eluent [CH_2Cl_2/MeOH = 9:1 (v/v)] and subjected to silica gel column chromatography. Fractions containing carboxy-CAP were combined and further purified by two rounds of semi-preparative HPLC purification. Finally, 15 mg of colorless powder were obtained from 5 liters of culture broth.

Time course of carboxy-CAP formation in *N. synnemataformans* culture supplemented with CAP: *N. synnemataformans* was inoculated into three 1 L-flasks with 250 mL of GYM-NaCl medium and cultures were incubated at 28 °C, 160 rpm. After 3–4 days, the three 1 L-flask cultures were combined and well mixed and then evenly distributed to three fresh sterilized 1 L-flasks. Subsequently, CAP was added to a final concentration of 12 μg/mL. The time at which CAP was added was defined as 0 h and at each time point (24, 48, 60, 72, 78, 84, 97 and 125 h) 2 mL supernatant were "harvested" by centrifugation and extracted with an equal volume of EtAOc/MeOH [9:1 (*v*/*v*)] + 1% AcOH. The solvents of 1 mL organic phase were removed in a Speedvac and residues were redissolved in 100 μL CH_3CN and then subjected to analytical HPLC. Experiments were performed in biological triplicates.

NMR spectroscopy: ^1H- and ^{13}C-NMR spectra were measured on a Bruker Avance III HD 400 instrument in CD_3CN (^1H: 400 MHz, ^{13}C: 100 MHz). Spectra were referenced to the residual solvent peak.

Agar diffusion assay: *N. synnemataformans*, *B. subtilis*, *M. luteus*, *E. coli*, *P. fluorescens* and *S. cerevisiae* were used as indicator organisms. *N. synnemataformans* was grown in GYM-NaCl medium at 28 °C for 4 days. *B. subtilis* and *E. coli* were grown in LB medium at 37 °C overnight to an OD_{600} of 1.1 and 1.0, respectively. *P. fluorescens* and *M. luteus* were grown in medium 1 (DMSZ) at 28 °C overnight and for 2 days to an OD_{600} of 1.1 and 1.4, respectively. *S. cerevisiae* was grown in medium 65 (DMSZ) at 28 °C overnight to an OD_{600} of 1.1. Each medium prepared with 1% agar was inoculated with 1% (v/v) relevant above indicator organism culture and dispensed into a petri dish. CAP and carboxy-CAP were dissolved in MeOH and pipetted onto sterilized filter paper disks on top of the solidified agar. A blank was prepared using MeOH only. Afterwards, the plates were incubated at 28 °C or 37 °C for 1 day (*B. subtilis*, *E. coli*, *P. fluorescens* and *S. cerevisiae*), 2 days (*M. luteus*) and 4 days (*N. synnemataformans*) to allow microbial growth. The activity was evaluated by zones of inhibition. All assays were performed at least in triplicates.

Minimum inhibitory concentration: Based on the time course of carboxy-CAP formation in the *N. synnemataformans* culture supple-

mented with CAP, *N. synnemataformans* was inoculated into two 1 L-flasks with 250 mL of GYM-NaCl medium and cultures were incubated at 28 °C, 160 rpm for 4 days. Then the cultures were combined and mixed and re-split to two fresh 1 L-flasks. Each flask containing 250 mL culture was treated with CAP (12 μg/mL, dissolved in EtOH) or an equal volume of EtOH. The two 1 L-flask cultures were incubated at 28 °C, 160 rpm for 60 h. The resulting cultures (25 μL) were pipetted into sterilized tubes 1–9 to determine the MIC of CAP for *N. synnemataformans*; CAP (dissolved in EtOH) and 4.943 mL of GYM-NaCl medium were well mixed and transferred to sterilized tubes 1–10 (Table S3). Tube 1 was set up as growth control and tube 10 was used as sterility control. The tubes were incubated at 28 °C, 160 rpm for additional 4 days. The minimum inhibitory concentration of CAP for *N. synnemataformans* was determined as the minimum concentration at which no *N. synnemataformans* growth could be detected by eye. Experiments were performed in biological triplicates.

Time course of carboxy-CAP formation by *N. synnemataformans* cell-free lysate obtained at different time points/growth stages: *N. synnemataformans* was inoculated into a 250 mL-flask with 50 mL GYM-NaCl medium and the culture was incubated at 28 °C, 160 rpm for 3–4 days. Then 5 mL of the pre-culture were transferred to two 2 L-flasks with 800 mL GYM-NaCl medium, each. After 24 h, the two 2 L-flask cultures were treated with either CAP (12 μg/mL, dissolved in EtOH) or the same amount of EtOH (defined as starting time point: 0 h). 100 mL culture were sacrificed after every 12 h by centrifugation at 18 000 g and 4 °C for 30 min. The cells were resuspended in lysis solution (50 mM sodium phosphate pH 7.2, 10% glycerol) supplemented with 1 mM phenylmethylsulfonyl fluoride (PMSF) and 1 mg/mL lysozyme, stirred at 4 °C for 30 min and lysed by ultrasonication (1 s pulse, 3 s pause; 3 min pulse time, 3 times) with a Branson Digital Sonifier. Cell debris was removed by centrifugation at 18 000 g (4 °C) for 30 min and the clear supernatant was filtered through a 0.45 μm syringe filter. A mixture of 125 μM CAP and 50 μM FAD was prepared in 50 mM sodium phosphate buffer (pH 7.2). The reaction was started by adding 45 μL cell-free lysate and samples were incubated at 28 °C and 500 rpm for 1 h. The reaction products were extracted with 1 mL EtOAc (+1% AcOH) and 500 μL of the organic phase was transferred into a 2.0 mL microcentrifuge tube and dried in a Speedvac. Finally, samples were redissolved in CH_3CN and analyzed by HPLC. Experiments were performed in three independent biological replicates.

HPLC detection: Samples were analyzed by reversed phase (RP) HPLC on a 1100 series chromatographic system (Agilent Technologies) with different columns. For analytical chromatography, a NUCLEODUR Sphinx RP or C18 Pyramid column (150×3 mm inner diameter (ID), 3 μm, Macherey-Nagel) coupled with a UNIVERSAL RP guard column (4×3 mm ID, Macherey-Nagel) was used. Separation was performed at 30 °C with a gradient elution (mobile phase A: water with 0.1% formic acid, mobile phase B: acetonitrile with 0.1% formic acid, the stepwise gradient: 10% B from 0 to 5 min, 10–58% B from 5 to 20 min, 58–95% B from 20 to 21 min, 95% B from 21 to 26 min, 95–10% B from 26 to 32 min). The flow rate was 1 mL/min and absorption changes were recorded at 254 nm as well as 280 nm, 350 nm and 450 nm. For semi-preparative chromatography (mobile phases were used as described above), a VP NUCLEODUR 100-5C18ec (250×10 mm ID, 5 μm, Macherey-Nagel) coupled with a UNIVERSAL RP guard column (4×3 mm ID, Macherey-Nagel) was used with a gradient elution (10% B from 0 to 2 min, 10–50% B from 2 to 5 min, 50–74% B from 5 to 12 min, 74–95% B from 12 to 13 min, 95% B from 13 to 20 min, 95–10% B from 20 to 26 min, the flow rate was 3 mL/min and absorption changes were recorded at 280 nm) at 30 °C as the first purification step. A VP NUCLEODUR C18 Gravity-SB column (250×10 mm ID, 5 μm, Macherey-Nagel) equipped with a UNIVERSAL RP guard column (4×3 mm ID, Macherey-Nagel) was used with an isocratic method (60% B for 12 min, the flow rate was 4 mL/min and absorption changes were recorded at 280 nm as well as 350 nm) at 30 °C as second purification step.

UPLC-HRMS analysis: UPLC-HRMS analyses were performed using a Waters ACQUITY I-class UPLC coupled with an ACQUITY UPLC photo diode array detector, and a Waters Synapt G2-Si quadrupole time-of-flight mass (Q-TOF) spectrometer equipped with an electrospray ionization (ESI) source. An analytical RP C18 column (ACQUITY UPLC HSS T3, 100 Å, 1.8 μm, 2.1×100 mm; Waters) was used at a flow rate of 0.2 mL/min with water+0.1% FA as mobile phase A and acetonitrile+0.1% FA as mobile phase B. The column was kept at 30 °C with following gradient: 10% B from 0 to 2 min, 10–95% B from 2 to 9 min, 95%B from 9 to 12 min, 95–10%B from 12 to 12.2 min, 10% B from 12.2 to 15 min. The samples of 2–10 μL were analyzed either in MS positive ion mode with a capillary voltage of 3.5 kV, 100 °C source temperature, 300 °C desolvation gas temperature and 800 L/h N_2 desolvation gas flow rate or in MS negative ion mode with a capillary voltage of 1.5 kV, 100 °C source temperature, 400 °C desolvation gas temperature and 800 L/h N_2 desolvation gas flow rate.

***N. synnemataformans* cell-free lysate assay**: Based on the time course of carboxy-CAP formation by *N. synnemataformans* cell-free lysate obtained at different time points, *N. synnemataformans* cells were harvested by centrifugation after 60 h of CAP treatment. Cell-free lysates were prepared as described above. For the assays under aerobic conditions, a mixture of 250 μM 2,6-dichlorophenyl indophenol (DCIP), 50 μM FAD and 125 μM CAP was prepared in 50 mM sodium phosphate buffer (pH 7.2). Then, the reactions were started by adding 45 μL active or heated (inactive) cell-free lysate and incubated at 28 °C while shaking at 500 rpm for 1 h. For the assays under anoxic conditions, the dioxygen in the mixture and active cell-free lysate were thoroughly removed by overnight incubation in an anoxic chamber. Subsequently, the reactions were started by adding 45 μL active cell-free lysate in the presence or absence of DCIP in the anoxic chamber and incubated at room temperature for 1 h. All the reactions were terminated by addition of 1 mL EtOAc (+1% AcOH) and 500 μL of the organic phase were transferred to a fresh 2.0 mL microcentrifuge tube. After drying in a Speedvac, residues were redissolved in CH_3CN and analyzed by HPLC and/or UPLC-HRMS.

Activity-guided purification of CAP-ADH from *N. synnemataformans* cell-free lysate: Native CAP-ADH was purified from *N. synnemataformans* cell-free lysate by sequential anion exchange chromatography (AEC), hydrophobic interaction chromatography (HIC) and size-exclusion chromatography (SEC). Fractions were screened for enzyme activity as described for *N. synnemataformans* cell-free lysate assay (see above) with each fraction instead of cell-free lysate.

For AEC, the *N. synnemataformans* cell-free lysate was prepared as described above in 9 mL of AEC buffer A (50 mM Tris, 10% glycerol, pH 7.2). The chromatographic separation was performed on an ÄKTA pure protein chromatography system (GE Healthcare) equipped with a 45 mL Q-Sepharose Fast Flow XK16/20 column at a flow rate of 5 mL/min. The column was pre-equilibrated with AEC buffer A and washed with 3 column volumes (CVs) of buffer A after loading. For elution, a linear gradient 0–100% AEC buffer B (buffer A+1 M NaCl, pH 7.2) within 3 CVs was applied, followed by an isocratic step (100% buffer B; 1 CV) and fractions of 10 mL were collected. The same AEC purification was performed three times and then the most active fractions were combined for HIC.

HIC was carried out using the same instrument equipped with a HiTrap Phenyl HP column (1 mL bed volume) pre-equilibrated with HIC buffer A (20 mM sodium phosphate buffer, 0.6 M ammonium sulfate, pH 7.2) at a flow rate of 1 mL/min. The AEC active combined fractions were concentrated, and buffer was exchanged to HIC buffer A using a 10 kDa MW cut-off MACROSEP spin column (Pall Cooperation). After sample application, the column was washed with 5 CVs of HIC buffer A. For elution, a linear gradient 0–100% HIC buffer B (20 mM sodium phosphate buffer, pH 7.2) within 5 CVs was applied, followed by an isocratic step (100% buffer B; 7 CVs) and fractions of 1 mL were collected. The most active fraction was prepared for SEC.

SEC was also carried out on the same instrument, utilizing a Superdex 200 10/300 GL column (24 mL bed volume) pre-equilibrated with SEC buffer (20 mM sodium phosphate buffer, pH 7.2) at a flow rate of 0.5 mL/min. The most active HIC fraction was directly load onto the column and proteins were eluted in SEC buffer with an isocratic run over 1.2 CVs (0.5 mL for each fraction). Because of the low amount of protein, direct determination of the concentration was not possible. Therefore, 400 µL of 2 active fractions, each, were precipitated with trifluoroacetic acid (TFA) at −20 °C for 5 min. After that, the protein solutions were incubated in the fridge overnight and then centrifuged at 13 000 rpm and 4 °C for 15 min. The supernatant was discarded and the pellets were washed with 200 µL ice-cold acetone. The pellets were then dissolved in 15 µL 1× loading buffer (ROTI®Load 1, ROTH Germany) and 1 µL separating gel buffer (1.5 M Tris, pH 8.8) prior to SDS-PAGE. Finally, based on the activity of each fraction, equal amounts of protein (15 µg) contained in *N. synnemataformans* cell-free lysate, AEC (1 fraction) and HIC (2 fractions) were subjected to SDS-PAGE and Coomassie brilliant blue staining to analyze the quality of the purification.

Protein identification by mass spectrometry of peptides: Proteins were identified by excising the bands of interest from SDS-PAGE gels. The bands were digested using trypsin and the resulting peptides were analyzed by UPLC-HRMS, coupled with a Synapt G2-Si electrospray ionization quadrupole time-of-flight (ESI-Q-TOF) mass spectrometry system (Waters); the system was described in detail by Mergelsberg et al.[33]

Verification of the function of recombinant CAP-ADHs: To verify the function of recombinant CAP-ADHs, fraction containing respective enzyme after each Ni-NTA HisTrap column purification was incubated with 200 µM CAP in the presence of 20 µM FAD at 30 °C and 500 rpm. After 10 min, all assays were quenched as described for *N. synnemataformans* cell-free lysate assay and analyzed by HPLC.

Gene cloning, heterologous production: CAP-ADH+^{NS}: The *cap-adh+^{NS}* gene (NCBI-accession number: WP_017563851.1) was amplified from genomic DNA of *N. synnemataformans* DSM 44143 (DMSZ) using the Q5 High-Fidelity 2× Master Mix (New England Biolabs) according to the manufacturer's protocols and then cloned into the pET28b vector (Novagen, Merck KgaA), in frame with the coding sequence for an N-terminal His_6-tag using Fast Digest BamHI and XhoI (Thermo Scientific). The successful insertion of the gene was confirmed by sequencing (Eurofins Genomic) and the recombinant plasmid was transformed into *E. coli* BL21 (DE3) cells (Thermo Scientific). For gene expression, TB-medium supplemented with kanamycin (50 µg/mL) was inoculated with a pre-culture grown in LB-medium (supplemented with the same amount of kanamycin) and incubated at 37 °C and 130 rpm until an OD_{600} of 0.6-0.8 was reached. Then, the temperature was set to 18 °C and protein production was induced by adding IPTG to a final concentration of 100 µM. After overnight incubation at 18 °C and 130 rpm, the cells were harvested by centrifugation (4 000 g for 15 min).

Gene cloning, heterologous production: CAP-ADH+^{NR}: In order to get a soluble and promising candidate for in-depth mechanistic studies, the *cap-adh+^{NR}* gene (NCBI-accession number: WP_047868087.1) codon optimized for *E. coli* was purchased from BioCat (Heidelberg, Germany), subcloned into the pET28b vector, in frame with the coding sequence for an N-terminal His_6-tag and codon optimized for *E. coli.* The recombinant plasmid was transformed into *E. coli* BL21 (DE3) cells for subsequent gene expression, which was performed as described for CAP-ADH+^{NS}. However, CAP-ADH+^{NR} produced using this strategy was poorly soluble. To increase the solubility of the enzyme, fusion with N-terminal solubility enhancer proteins was tested. Therefore, an overlap PCR was performed using two pairs of primers (Table S8), Fwd. 1 and Rev. 1, for the 5′ and 3′ ends of the *cap-adh+^{NR}* gene; Fwd. 2 and Rev. 2, that bind at the NcoI restriction site for the purpose of mutating one base pair. Two separate PCR mixtures were made combining the Fwd. 1 and Rev. 2 and the Fwd. 2 and Rev. 1 to produce two fragments. After gel clean-up by QIAquick PCR & Gel clean up Kit (QIAGEN), the two fragments were combined in another PCR reaction. Finally, the mutated *cap-adh+^{NR}* gene was digested with Fast Digest NcoI and NotI (Thermo Fisher) and cloned into the pET-M11-His-TEV vector, containing either the coding sequence for the solubility enhancer protein GB1 (B1-domain of protein G) or for MBP (maltose binding protein) between the nucleotides encoding the His6-tag and the tobacco etch virus (TEV)-cleavage site. The plasmids were separately transformed into *E. coli* BL21 plus RP pL1SL2 (2) cells, which contain *Streptomyces coelicolor* chaperonins (GroEL1, GroEL2 and GroES) to increase the solubility of the recombinant proteins.[18]

For gene expression, TB-medium supplemented with kanamycin (50 µg/mL), ampicillin (100 µg/mL), CAP (20 µg/mL) and 0.2% glucose was inoculated with a pre-culture grown in LB-medium (supplemented with the same amount of antibiotics) and incubated at 37 °C and 130 rpm until an OD_{600} of 0.6-0.8 was reached. Then, the temperature was set to 18 °C and protein production was induced by adding IPTG to a final concentration of 100 µM. After overnight incubation at 18 °C and 130 rpm, the cells were harvested by centrifugation (4 000 g for 15 min).

Protein purification: CAP-ADH+^{NR}: For protein purification, cells were treated as described for CAP-ADH+^{NS}. For GB1-CAP-ADH+^{NR}, the corresponding supernatant was filtered through a 0.45 µM syringe filter before loading it onto a 5 mL Ni-NTA HisTrap HP column (GE healthcare, Cytiva) pre-equilibrated with buffer A. Unspecifically bound protein was removed by washing with 4% buffer B and GB1-CAP-ADH+^{NR} was eluted by an isocratic elution with 100% buffer B over 6 CVs. For MBP-CAP-NH^{NR}, the corresponding supernatant was filtered through a 0.45 µM syringe filter before loading it onto a 5 mL MBP-trap column (GE healthcare, Cytiva) pre-equilibrated with buffer A. Unspecifically bound protein was removed by washing with about 10 CVs of buffer A and the MBP-CAP-ADH+^{NR} was eluted by gradient elution from 0% to 100% buffer C (50 mM sodium phosphate, 300 mM NaCl, 10 mM maltose, 10% glycerol, pH 7.2) over 6 CVs. The identity and purity of the eluted proteins was confirmed by SDS-PAGE. GB1-CAP-ADH+^{NR} was still poorly soluble but the amount of protein was sufficient for enzyme characterization. MBP-CAP-NH^{NR}, in contrast, was inactive despite better solubility. Therefore, only GB1-CAP-ADH+^{NR} (~ 10 µM) was flash frozen in liquid N_2 and stored at −80 °C for further use.

Gene cloning, heterologous production: CAP-ADH+^{SY}: In order to get a soluble and promising candidate for in-depth mechanistic studies, the *cap-adh+^{SY}* gene (NCBI-accession number: WP_119287296.1) codon optimized for *E. coli* was purchased from BioCat (Heidelberg, Germany), subcloned into the pET28b vector, in frame with the coding sequence for a C-terminal His_6-tag. The

plasmid was transformed into *E. coli* BL21 (DE3) for subsequent gene expression, which was performed as described for CAP-ADH+^{NS}. However, CAP-ADH+^{SY} was also poorly soluble. Again, to increase the solubility of the protein, the gene was re-cloned into the pET–M11-His-TEV vector containing a coding sequence for either a GB1- or an MBP-tag between the nucleotide sequence encoding the His_6-tag and the TEV-cleavage site after restriction digestion with NcoI (5′) and NotI (3′). The plasmids were then separately transformed into *E. coli* BL21 plus RP pL1SL2 cells as described for CAP-ADH+^{NR}.

Protein purification: CAP-ADH+^{SY}: For protein purification, cells were treated as described for CAP-ADH+^{NR}. Like GB1-CAP_DH^{NR}, GB1-CAP-ADH+^{SY} was still poorly soluble, but again enough protein for enzyme characterization could be obtained. MBP-CAP-ADH+^{SY} like MBP-CAP_DH^{NR} was inactive despite its improved solubility.

Gene cloning, heterologous production: CAP-ADH-^{SC}: In order to verify the function of CAP-ADH-^{SC}, the respective gene (NCBI-accession number: WP_155178455.1) codon optimized for *E. coli* was purchased from BioCat, subcloned into the pET28b vector, in frame with the coding sequence for an N-terminal His_6-tag. The plasmid was transformed into *E. coli* BL21 (DE3) cells for subsequent gene expression, which was performed as described for CAP-ADH+^{NS}.

Protein purification: CAP-ADH-^{SC}: For the affinity purification with Ni-NTA HisTrap HP column, cells were treated as described for CAP-ADH+^{NS}. The protein containing fractions were pooled and concentrated for further purification with SEC utilizing a HiLoad 16/600 Superdex 200 pg column (GE Healthcare) pre-equilibrated with buffer (50 mM sodium phosphate, 50 mM NaCl, 10 μM FAD, 5% glycerol, pH 7.2). The identity and purity of the eluted protein was confirmed by SDS-PAGE. Aliquots of purified octameric protein [Note: the octamer is able to catalyze carboxy-CAP formation, the monomer, however, cannot convert CAP to carboxy-CAP] were flash frozen in liquid N_2 prior to storage at −80 °C.

Gene cloning, heterologous production: CAP-ADH-^{NB} and CAP-ADH-^{SA}: In order to get promising candidates for in-depth mechanistic studies, the *cap-adh-*^{NB} and *cap-adh-*^{SA} genes (NCBI-accession number: WP_088308422.1 and WP_161828970.1) codon optimized for *E. coli* were purchased from BioCat, subcloned into the pET28b vector, in frame with the coding sequence for a C-terminal His_6-tag. The plasmids were separately transformed into *E. coli* BL21 (DE3) cells for subsequent gene expression, which was carried out as described for CAP-ADH+^{NS}.

For protein crystallization, the *cap-adh-*^{NB} gene was re-cloned into the pET–M11-His-TEV vector (N-terminal His_6 tag) after restriction digestion with NcoI (5′) and NotI (3′). To remove the C-terminal His_6 tag from the *CAP-ADH-*^{NB} gene, a PCR-based mutagenesis was performed using oligonucleotides synthesized by Sigma-Aldrich (Table S8). First, amplification over 10 cycles of pET-M11-His-TEV-*CAP-ADH-*^{NB} (N&C-terminal His_6 tag) using separate reactions with forward and reverse primers was performed using the Q5 High-Fidelity 2× Master Mix according to the manufacturer's protocols. The "forward" and "reverse" reactions were then combined for further 30 cycles. The resulting PCR product was purified using QIAquick PCR Purification Kit (QIAGEN) prior to digestion with Fast Digest DpnI (New England Biolabs) at 37 °C for 2 h to remove template plasmid. Successful generation of the pET-M11-His-TEV-*CAP-ADH-*^{NB} (N-terminal His_6 tag) construct was confirmed by sequencing, before transforming it into *E. coli* BL21 (DE3) cells. Gene expression was carried out as described for CAP-ADH+^{NS}.

Protein purification: CAP-ADH-^{NB} and CAP-ADH-^{SA}: The protein (octamers) purifications of CAP-ADH-^{NB} and CAP-ADH-^{SA} were carried out as described for CAP-ADH-^{SC}. For proteins used for subsequent crystallization experiments, the cells containing protein CAP-ADH-^{NB} (N-terminal His_6 tag) were treated as described for CAP-ADH+^{NS} in buffer D (50 mM potassium phosphate, 300 mM KCl, 10 μM FAD, 10% glycerol, pH 6.8). Subsequently, the supernatant was loaded onto a 5 mL Ni-NTA HisTrap FF crude column (GE healthcare, Cytiva) pre-equilibrated with buffer D. Unspecifically bound protein was removed by washing with 4% buffer E (50 mM potassium phosphate, 300 mM KCl, 500 mM imidazole, 10% glycerol, pH 6.8). CAP-ADH-^{NB} was eluted by gradient elution from 4% to 100% buffer E over 6 CVs. Protein (monomer) containing fractions were pooled and incubated with TEV-protease (10:1, m/m) overnight at 4 °C. The His-tag and TEV-protease were removed by a second round of affinity chromatography. CAP-ADH-^{NB} was eluted in the flow through fraction and applied to a HiLoad 16/600 Superdex 200 pg column pre-equilibrated with buffer F (50 mM potassium phosphate, 50 mM KCl, 10 μM FAD, pH 6.8). The identity and purity of the eluted protein was confirmed by SDS-PAGE. Again, fractions containing monomeric protein were pooled and concentrated to ~218 μM (~13 mg/mL) and FAD was added to a final concentration of 0.6 mM. Aliquots were prepared and flash frozen in liquid N_2 prior to storage at -80 °C until further use.

CAP-ADH+^{NS} catalyzed carbxy-cap formation in the presence or absence of CAP-ALDH^{SC}: To check the role of CAP-ALDH^{SC} in the formation of carboxy-CAP catalyzed by CAP-ADH+^{NS}. A fraction containing CAP-ADH+^{NS} after Ni-NTA HisTrap column purification was incubated with 200 μM CAP, 30 μM FAD in the presence or absence of 3 μM CAP-ALDH^{SC} and 10 μM $NADP^+$ at 30 °C and 500 rpm. After 10 min, all assays were quenched as described for *N. synnemataformans* cell-free lysate assay and analyzed by HPLC.

CAP-ADH+^{NR} catalyzed carbxy-CAP formation in the presence or absence of CAP-ALDH^{SC}/DCIP: To check the role of CAP-ADH^{SC}/DCIP in the formation of carboxy-CAP catalyzed by CAP-ADH+^{NR}. The 200 μM CAP was incubated with 20 μM FAD and 1 μM CAP-ADH+^{NR} in the presence of 3 μM CAP-ALDH^{SC} and 10 μM $NADP^+$ or 400 μM DCIP at 30 °C and 500 rpm. After 10 min, all assays were quenched as describes for *N. synnemataformans* cell-free lysate assay and analyzed by HPLC.

Gene cloning, heterologous production: CAP-ALDH^{SC}: To verify the function of CAP-ALDH^{SC}, the *cap-aldh*^{SC} gene (NCBI-accession number: WP_155178457.1) codon optimized for *E. coli* was purchased from Biocat, subcloned into the pET28b vector, in frame with the coding sequence for a C-terminal His_6-tag. The plasmid was transformed into *E. coli* BL21 (DE3) cells for subsequent gene expression, which was performed as described for CAP-ADH+^{NS}.

Protein purification: CAP-ALDH^{SC}: For protein purification, cells were treated as described for CAP-ADH+^{NS} in buffer G (50 mM sodium phosphate, 300 mM NaCl, 10% glycerol, pH 7.2). The clear supernatant was filtered through a 0.45 μM syringe filter before loading it onto a 5 mL Ni-NTA HisTrap HP column pre-equilibrated with buffer G. Unspecifically bound protein was removed by washing with 8% buffer B. Subsequently, CAP-ALDH^{SC} was eluted by an isocratic elution with 100% buffer B over 6 CVs. The fraction containing the highest concentration of CAP-ALDH^{SC} was directly loaded onto a HiLoad 16/600 Superdex 200 pg column pre-equilibrated with buffer (50 mM Tirs, 100 mM NaCl, 5% glycerol, pH 7.4) for further purification. The identity and purity of the eluted protein was confirmed by SDS-PAGE. The fractions containing CAP-ALDH^{SC} were pooled and concentrated (NOTE: the protein precipitated while concentrating). The clear supernatant was collected (~30 μM) and flash frozen in liquid N_2 prior to storage at −80 °C until further use.

Enzymatic assays with CAP-ADH+^{NR}/CAP-ADH-^{NB}: Reaction mixtures containing 400 μM DCIP (only for CAP-ADH+^{NR}) and 60 μM FAD in 20 mM sodium phosphate buffer (pH 7.2) were well mixed with 3 μM CAP-ADH+^{NR}/ CAP-ADH-^{NB} and incubated at 30 °C and 500 rpm. After 4 min, 200 μM of CAP, thiamphenicol (TAP), florfenicol (FF) or AAF (azidamfenicol) of were added to start the assays. The reactions were stopped by either adding EtOAc (+1% AcOH) or MeOH (only for AAF). For the assays with CAP, TAP, and FF, the organic layers were transferred to fresh tubes and solvents were removed in a Speedvac. The residues were redissolved in CH_3CN and samples were analyzed by HPLC or UPLC-HRMS. The MeOH-containing samples (from AAF assays) were subjected to UPLC-HRMS analysis right after filtering through a 0.45 μM syringe filter.

$^{18}O_2$ labelling assay: The dioxygen in *N. synnemataformans* cell-free lysate; CAP-ADH+^{NR}; CAP-ADH-^{NB}; CAP-ALDH^{SC} and the assay mixtures containing 10 μM $NADP^+$ (only for CAP-ALDH^{SC}), 400 μM DCIP (only for CAP-ADH+^{NR}), 50 μM FAD and 200 μM CAP in 20 mM sodium phosphate buffer (pH 7.2) were thoroughly removed by overnight incubation in an anaerobic chamber. For *N. synnemtaformans* cell-free lysate, 90 μL of it was added to the pre-prepared mixture in the anaerobic chamber. Subsequently, about 1 mL 97% $^{18}O_2$ gas (Campro Scientific) was injected into reaction tube by a syringe and the assay was incubated at room temperature for 2 h.

For CAP-ADH+^{NR} or CAP-ADH-^{NB}, 3 μM of each enzyme were added to the pre-prepared mixture, either "alone" or together with 3 μM CAP-ALDH^{SC}, still kept in the anaerobic chamber. Subsequently, about 1 mL 97% $^{18}O_2$ gas (Campro Scientific) was injected into each reaction tube and the assays were incubated at room temperature for 10 min. Reaction products were extracted with 1 mL of EtOAc (+1% AcOH) and solvents were removed in the Speedvac. The residues were redissolved in CH_3CN and analyzed by UPLC-HRMS.

$H_2{}^{18}O$ labelling assay: Assays were performed in reaction mixtures containing 50% (v/v) of $H_2{}^{18}O$, 10 μM $NADP^+$ (only for CAP-ALDH^{SC}), 400 μM DCIP (only for CAP-ADH+^{NR}), 50 μM FAD and 200 μM CAP in 20 mM sodium phosphate buffer (pH 7.2). For the assay with *N. synnemataformans* cell-free lysate, 90 μL of it was added to the reaction mixture under aerobic condition and incubated at 30 °C and 500 rpm for 2 h. For the assays with CAP-ADH+^{NR} or CAP-ADH-^{NB}, 3 μM of each enzyme were added to reaction mixture either "alone" or together with 3 μM CAP-ALDH^{SC} under aerobic condition. The assays were incubated at 30 °C and 500 rpm for 10 min. The reaction products were treated as described for the $^{18}O_2$ labelling experiment.

Time course of carboxy-CAP formation by CAP-ADH+^{NR}/CAP-ADH-^{NB} in the presence or absence of DCIP and/or ferricyanide: To study the time-dependent formation of carboxy-CAP by CAP-ADH+^{NR}/CAP-ADH-^{NB}, the reaction mixtures containing 20/60 μM FAD, 600 μM DCIP and/or potassium ferricyanide (only for CAP-ADH-^{NB}), 1 μM CAP-ADH+^{NR}/3 μM CAP-ADH-^{NB} in 20 mM sodium phosphate buffer (pH 7.2) were incubated at 30 °C and 500 rpm for 4 min. To start the assays, 300 μM CAP were added and 100 μL of sample were withdrawn from each tube and quenched with EtOAc +1% AcOH (1 mL) after 0, 10, 30, 120, 300, 600 and 1200 s. The organic layers were transferred to fresh microcentrifuge tubes and dried in a Speedvac. The residues were redissolved in CH_3CN for subsequent HPLC-DAD analysis. For all assays, three independent replicates were prepared and analyzed.

Time course of carboxy-CAP formation by *N. synnemtaformans* cell-free lysate in the presence or absence of DCIP: To study the time-dependent formation of carboxy-CAP by *N. synnemataformans* cell-free lysate, reaction mixtures containing 50 μM FAD, 600 μM DCIP, 45 μL of *N. synnemataformans* cell-free lysate in 20 mM sodium phosphate buffer (pH 7.2) were incubated at 30 °C and 500 rpm for 4 min. Subsequently, the assays were started by adding 300 μM CAP and the following procedures were performed as described for time course of carboxy-CAP formation by CAP-ADH+^{NR}/CAP-ADH-^{NB} (see above) with quenching after 0, 5, 10, 30 and 60 min.

Time course of carboxy-CAP formation by CAP-ADH-^{SC} in the presence or absence of DCIP and/or CAP-ALDH^{SC}: To study the time-dependent formation of carboxy-CAP by CAP-ADH-^{SC}, the reaction mixtures containing 0.5 μM CAP-ADH-^{SC}, 10 μM FAD, 1.5 mM DCIP and/or 2 μM CAP-ALDH^{SC} and 10 μM $NADP^+$ in 20 mM sodium phosphate buffer (pH 7.2) were incubated at 30 °C and 500 rpm for 4 min. To start the assays, 750 μM CAP were added and the following procedures were carried out as describe for time course of carboxy-CAP formation by CAP-ADH+^{NR}/CAP-ADH-^{NB} (see above) with quenching after 0, 20, 60, 120, 300 and 600 s.

Enzyme characterization of CAP-ADH-^{SC}/CAP-ADH-^{NB}/CAP-ADH+^{NR}: To determine the temperature optimum, reaction mixtures containing 10 or 60 μM FAD, 500 μM DCIP (for CAP-ADH-^{SC} and CAP-ADH+^{NR}) and 0.5 μM CAP-ADH-^{SC}/3 μM CAP-ADH-^{NB}/0.5 μM CAP-ADH+^{NR} in 20 mM sodium phosphate buffer (pH 7.2) were incubated at different temperatures (20-60 °C) and 500 rpm for 4 min. The reactions were then started by adding CAP to a final concentration of 250 μM and further incubated for 1 min (for CAP-ADH-^{SC} and CAP-ADH+^{NR}) or 2 min (for CAP-ADH-^{NB}). The assays were quenched and extracted with 1 mL of EtOAc (+1% AcOH) and solvents were removed in a Speedvac. The residues were redissolved in CH_3CN and samples were analyzed by HPLC-DAD.

To determine the pH optimum, the reaction mixtures containing 10 or 60 μM FAD, 0.5 μM CAP-ADH-^{SC}/3 μM CAP-ADH-^{NB}/0.5 μM CAP-ADH+^{NR}, 500 μM DCIP (for CAP-ADH-^{SC} and CAP-ADH+^{NR}) in buffers (Table S12) were incubated at 30 °C and 500 rpm. After 4 min, the assays were started by the addition of 250 μM CAP and incubated under the same conditions for 1 min (for CAP-ADH-^{SC} and CAP-ADH+^{NR}) or 2 min (for CAP-ADH-^{NB}). The reaction products were extracted with 1 mL of EtOAc (+1% AcOH) and solvents were removed in a Speedvac. The residues were redissolved in CH_3CN and subjected to HPLC-DAD analysis. For all assays, three independent replicates were prepared and analyzed.

CAP-ADH-^{NB} catalyzed carboxy-CAP and CAP-aldehyde formation in the presence or absence of CAP-ALDH^{SC} under aerobic and anoxic conditions: To characterize the influence of CAP-ALDH^{SC} in the formation of carboxy-CAP and CAP-aldehyde by CAP-ADH-^{NB} under aerobic and anoxic conditions. For aerobic conditions, 250 μM CAP was incubated with 3 μM CAP-ADH-^{NB} and 60 μM FAD in the presence or absence of 3 μM CAP-ALDH^{SC} and 10 μM $NADP^+$ at room temperature. For anoxic conditions, assays were performed as described above before the dioxygen in the all components were removed as described for $^{18}O_2$ labelling assay. After 10 min, all assays were quenched as described for the *N. synnemataformans* cell-free lysate assay and analyzed by HPLC or UPLC-HRMS.

CAP-ADH-^{NB} monomer assay: To determine the activity of the monomeric CAP-ADH-^{NB}, 200 μM CAP were incubated with 30 μM of CAP-ADH-^{NB} in the presence or absence of 3 μM CAP-ALDH^{SC} and 10 μM $NADP^+$ in 50 mM potassium phosphate (pH 6.8) at 30 °C for 30 min. The reaction products were extracted with 1 mL EtOAc (+1% AcOH) and solvents were removed in a Speedvac. For a negative control, CAP-ADH-^{NB} was replaced with same volume of buffer F. The residues were dissolved in CH_3CN and analyzed by HPLC-DAD and UPLC-HRMS.

Site-directed mutagenesis: In order to generate the *CAP-ADH-^{NB}*-His471 variant, the required nucleotide substitutions were intro-

duced into the pET28b-*CAP-ADH-*^{NB} wild type expression plasmid by PCR-based mutagenesis using oligonucleotides synthesized by Sigma-Aldrich (Table S8). First, amplification over 10 cycles using separate reactions with forward and reverse primers, respectively, was performed using the Q5 High-Fidelity 2X Master Mix according to the manufacturer's protocols. The forward and reverse reactions were then combined for further 30 cycles. PCR products were purified using QIAquick PCR Purification Kit (QIAGEN) before digesting them with FastDigest DpnI (New England Biolabs) at 37 °C for 2 h to remove template plasmid. After transformation of *E. coli* TOP10 cells and amplification of the modified plasmid, plasmid DNA was isolated and the mutation confirmed by sequencing. The construct was then transformed into *E. coli* Bl21 (DE3) cells for protein production, before the enzyme variant was purified, as described for octameric CAP-ADH-^{NB} wild type with slight modification (see above). Briefly, the HiLoad 16/600 Superdex 200 pg column was replaced by a Superdex 200 10/300 GL column during SEC purification.

CAP-ADH-^{NB} variants enzyme assay: To compare the activity of CAP-ADH-^{NB} variants with the wild type enzyme, all assays were performed as described for enzyme characterization of CAP-ADH-^{NB} with CAP.

CAP-ADH-^{SC}/CAP-ADH-^{NB}/CAP-ADH+^{NR} substrate specificity and steady-state kinetic: Steady-state parameters for the oxidation of CAP by CAP-ADH-^{SC}/CAP-ADH-^{NB}/CAP-ADH+^{NR} were determined using a T80+ UV/VIS Spectrometer (PG Instruments Ltd), in a coupled assay with DCIP or potassium ferricyanide. Reaction mixtures containing 1/2.5 μM FAD, 150 μM DCIP and 50 nM CAP-ADH-^{SC}/125 nM CAP-ADH+^{NR} were incubated at 30 °C for 4 min and then transferred to a 10 mm PS semi-micro cuvette (ratiolab). Subsequently, the reaction was started by adding varying final concentrations of CAP (2.5–300 μM/2.5-600 μM) or TAP (2.5-750 μM) and absorbance changes at 700 nm were continuously monitored for 130 s (NOTE: for CAP-ADH-^{NR} catalyzed oxidation of TAP, the consumption of DCIP could not be accurately determined). Similarly, reaction mixtures containing 24 μM FAD, 600 μM potassium ferricyanide and 1.2 μM CAP-ADH-^{NB} were incubated at 30 °C for 4 min and then transferred to a 10 mm PS semi-micro cuvette. To start the reactions, varying final concentrations of CAP (10 to 600 μM) or TAP (10 to 750 μM) were added and absorbance changes at 420 nm were recorded for 130 s. Apparent k_{cat} and K_M values were calculated based on the Lambert-Beer's law using the extinction coefficients of DCIP (700 nm) and potassium ferricyanide (420 nm), which were calculated to 5518 $M^{-1}cm^{-1}$ and 1050 $M^{-1}cm^{-1}$ at pH 7.2, respectively. For all assays, three independent replicates were prepared and analyzed.

Phylogenetic tree: A phylogenetic distance tree of GMC-family flavoenzymes and CAP-ADHs with indicated bootstrap values (2000 replicates) was generated with the MEGA X software using the maximum likelihood method and JTT matrix-based model.[34] Amino acid sequences were aligned using the ClustalW algorithm. The phylogenetic tree was visualized and color-edited using MEGA X or the online program iTOL.[35]

Determination of the molar extinction coefficient of CAP-ADH-^{NB}-bound FAD: To determine the molar extinction coefficient of the FAD-cofactor bound to CAP-ADH-^{NB}, UV-visible absorption spectra of the native protein solution (in 50 mM HEPES, 50 mM NaCl, 5% glycerol, pH 6.6) as well as of the enzyme denatured with 0.5% SDS were recorded between 300 and 800 nm. By assuming that the molar extinction coefficient of the FAD cofactor in the denatured protein sample equals the one of free FAD (ε_{450}: 11 300 $M^{-1}cm^{-1}$), the extinction coefficient of CAP-ADH-^{NB}-bound FAD at 450 nm was calculated to ~15 600 $M^{-1}cm^{-1}$.

Crystallization, data collection and structure determination of CAP-ADH-^{NB}: CAP-ADH-^{NB} crystals were grown in sitting-drop vapor diffusion set-ups (MRC 3 well – Polystyrene; SwissSci) at room temperature. Plate like protein crystals were obtained after mixing 0.2 μL of 218 μM (~13 mg/ml) protein solution in 50 mM potassium phosphate, 50 mM KCl, pH 6.8 with 0.2 μL of a complex reservoir solution (Solution D3 from Morpheus® crystallization screen,[36] Molecular Dimensions, Sheffield, UK). Crystals were directly flash cooled in liquid nitrogen. Data of a single crystal was collected at the SLS beamline X06SA (Swiss Light Source, Paul Scherrer Institute, Switzerland) at 100 K and were integrated, indexed using XDS software and scaled using AIMLESS.[38] The phase problem was solved using molecular replacement with an AlphaFold2 protein model.[22] Based on this replacement solution, manual model building and structure refinement were performed with Coot[39] and PHENIX.[40] Of the 539 amino acids, 458 residues could be built, loop residues aa42-56, aa91-95, aa134-153, aa299-333, and aa364-376 are missing in the final model. Model quality was validated with Molprobity.[41] Data collection and refinement statistics are summarized in Table S16. The atomic coordinates and structure factors have been deposited in the Protein Data Bank under the accession code 8B7S.

Proteomics: The *N. synnemataformans* cells were collected based on the time course of carboxy-CAP formation by *N. synnemataformans* cell-free lysate at different time points. For the negative control groups, the cells treated with CAP (final concentration of 12 μg/ml) and equal volume of EtOH at time 0 h were harvested by centrifugation at 4 °C and 18 000 g for 30 min, respectively. For the positive assay groups, the cells were harvested after 60 h of CAP and EtOH treatment by centrifugation at 4 °C and 18 000 g for 30 min, respectively. Cell-free lysates were prepared as described for N. *synnemataformans* cell-free lysate assay in the absence of 1 mg/mL lysozyme. The activity of each cell-free lysate was determined. The specific activities of both groups were 0.004, 0.005, 0.039 and 0.036 nmol min^{-1} mg^{-1}, respectively.

For each sample, 50 μg protein lysate was overnight precipitated with 5× volume ice-cold acetone at −20 °C. Protein pellets were obtained after 10 min centrifugation at 4 °C and 10 000 g. The protein lysate was loaded on SDS-gel and run for 10 min. The gel piece was cut, washed and incubated with 25 mM 1,4 dithiothreitol (in 20 mM ammonium bicarbonate) for 1 h and 100 mM iodoacetamide (in 20 mM ammonium bicarbonate) for 30 min, and destained, dehydrated and proteolytically cleaved overnight at 37 °C with trypsin (Promega). The digested peptides were extracted and desalted using ZipTip μC18 tips (Merck Millipore, Darmstadt, Germany). The peptide lysates were re-suspended in 15 μL 0.1% formic acid and analyzed by nanoliquid chromatography mass spectrometry (UltiMate 3000 RSLCnano, Dionex, Thermo Fisher Scientific). Mass spectrometric analyses of eluted peptide lysates were performed on a Q Exactive HF mass spectrometer (Thermo Fisher Scientific) coupled with a TriVersa NanoMate (Advion, Ltd., Harlow, UK). Peptide lysates were injected on a trapping column (Acclaim PepMap 100 C18, 3 μm, nanoViper, 75 μm × 2 cm, Thermo Fisher Scientific) with 5 μL/min by using 98% water/2% ACN 0.5% trifluoroacetic acid, and separated on an analytical column (Acclaim PepMap 100 C18, 3 μm, nanoViper, 75 μm × 25 cm, Thermo Fisher Scientific) with a flow rate of 300 nL/min. Mobile phase was 0.1% formic acid in water (A) and 80% ACN/0.08% formic acid in water (B). Full MS spectra (350–1,550 m/z) were acquired in the Orbitrap at a resolution of 120,000 with automatic gain control (AGC) target value of 3×10^6 ions.

The acquired MS data were analyzed with the Proteome Discoverer (v.2.5, Thermo Fischer Scientific) using SEQUEST HT, Inferys Rescoring and Percolator. The *.fasta protein-coding database was downloaded from UniProt (*Nocardiopsis dassonvillei*, reference

numbers: UP000002219) supplemented with common contaminant protein sequences (e.g. keratins and trypsin) and the target protein GMC family oxidoreductase [WP_017563851.1 from *Nocardiopsis synnemataformans*]. Database searches were conducted with the following parameters: Trypsin as enzyme specificity and two missed cleavages allowed. A peptide ion tolerance of 10 ppm and an MS/MS tolerance of 0.02 Da were used. As modifications, oxidation (methionine) and carbamidomethylation (cysteine) were selected. Peptides that scored a q-value $>1\%$ based on a decoy database and with a peptide rank of 1, were considered identified.

Acknowledgements

This work was supported by the Deutsche Forschungsgemeinschaft (DFG) by grant nos. TE 931/3-1, TE 931/4-1 (awarded to R.T.), by the Fonds zur Förderung der wissenschaftlichen Forschung (FWF) via an Erwin-Schrödinger stipend (J 4482-B) awarded to M.T., and by a Chinese Scholarship Council (CSC) grant 201706300026 awarded to L.Z. M.vB. is thankful for support by Novo Nordisk Foundation grant NNF21OC0066551. M.vB. and N.J. are grateful for funding of the UFZ for the ProMetheus platform for proteomics and metabolomics. We thank Jonathan Fuchs and the group of Matthias Boll for technical support. We thank the staff at the Swiss Light Source (Villigen, Switzerland) for support for crystallographic data collection at beamline PXI.

Conflict of Interest

The authors declare no conflict of interest.

Data Availability Statement

The data that support the findings of this study are available in the supplementary material of this article.

Keywords: antibiotics · antimicrobial resistance · bioremediation · chloramphenicol · flavoprotein dehydrogenases

[1] C. Antimicrobial Resistance, *Lancet* **2022**.
[2] a) H. J. Balbi, *Pediatr. Rev.* **2004**, *25*, 284–288; b) S. Schwarz, C. Kehrenberg, B. Doublet, A. Cloeckaert, *FEMS Microbiol. Rev.* **2004**, *28*, 519–542.
[3] L. T. Fernandez-Martinez, C. Borsetto, J. P. Gomez-Escribano, M. J. Bibb, M. M. Al-Bassam, G. Chandra, M. J. Bibb, *Antimicrob. Agents Chemother.* **2014**, *58*, 7441–7450.
[4] a) W. Tao, M. H. Lee, J. Wu, N. H. Kim, J. C. Kim, E. Chung, E. C. Hwang, S. W. Lee, *Appl. Environ. Microbiol.* **2012**, *78*, 6295–6301; b) A. Marchese, E. A. Debbia, E. Tonoli, L. Gualco, A. M. Schito, *J. Chemother.* **2002**, *14*, 554–561; c) G. P. Dinos, C. M. Athanassopoulos, D. A. Missiri, P. C. Giannopoulou, I. A. Vlachogiannis, G. E. Papadopoulos, D. Papaioannou, D. L. Kalpaxis, *Antibiotics* **2016**, *5*.
[5] C. S. Toro, S. R. Lobos, I. Calderon, M. Rodriguez, G. C. Mora, *Antimicrob. Agents Chemother.* **1990**, *34*, 1715–1719.
[6] a) J. A. Dunkle, L. Xiong, A. S. Mankin, J. H. Cate, *Proc. Natl. Acad. Sci. USA* **2010**, *107*, 17152–17157; b) D. Bulkley, C. A. Innis, G. Blaha, T. A. Steitz, *Proc. Natl. Acad. Sci. USA* **2010**, *107*, 17158–17163.
[7] a) M. Braibant, J. Chevalier, E. Chaslus-Dancla, J. M. Pages, A. Cloeckaert, *Antimicrob. Agents Chemother.* **2005**, *49*, 2965–2971; b) I. Roca, S. Marti, P. Espinal, P. Martinez, I. Gibert, J. Vila, *Antimicrob. Agents Chemother.* **2009**, *53*, 4013–4014; c) C. Kehrenberg, S. Schwarz, *Antimicrob. Agents Chemother.* **2004**, *48*, 615–618.
[8] I. A. Murray, W. V. Shaw, *Antimicrob. Agents Chemother.* **1997**, *41*, 1–6.
[9] R. H. Mosher, N. P. Ranade, H. Schrempf, L. C. Vining, *J. Gen. Microbiol.* **1990**, *136*, 293–301.
[10] T. S. Crofts, P. Sontha, A. O. King, B. Wang, B. A. Biddy, N. Zanolli, J. Gaumnitz, G. Dantas, *Cell Chem. Biol.* **2019**, *26*, 559-570 e556.
[11] a) G. Gadda, *Biochemistry* **2012**, *51*, 2662–2669; b) C. Martin, C. Binda, M. W. Fraaije, A. Mattevi, *Enzymes* **2020**, *47*, 63–86.
[12] T. Bennur, A. R. Kumar, S. Zinjarde, V. Javdekar, *Microbiol. Res.* **2015**, *174*, 33–47.
[13] L. Zhang, L. A. Esquembre, S. N. Xia, F. Oesterhelt, C. C. Hughes, H. Brotz-Oesterhelt, R. Teufel, *ACS Chem. Biol.* **2022**.
[14] a) M. G. Hvenegaard, B. Bang-Andersen, H. Pedersen, M. Jorgensen, A. Puschl, L. Dalgaard, *Drug Metab. Dispos.* **2012**, *40*, 1357–1365; b) W. P. Dijkman, G. de Gonzalo, A. Mattevi, M. W. Fraaije, *Appl. Microbiol. Biotechnol.* **2013**, *97*, 5177–5188; c) M. Pickl, M. Fuchs, S. M. Glueck, K. Faber, *Appl. Microbiol. Biotechnol.* **2015**, *99*, 6617–6642.
[15] R. Teufel, C. Gantert, M. Voss, W. Eisenreich, W. Haehnel, G. Fuchs, *J. Biol. Chem.* **2011**, *286*, 11021–11034.
[16] a) R. Teufel, V. Agarwal, B. S. Moore, *Curr. Opin. Chem. Biol.* **2016**, *31*, 31–39; b) R. Teufel, *Arch. Biochem. Biophys.* **2017**, *632*, 20–27; c) P. Chaiyen, M. W. Fraaije, A. Mattevi, *Trends Biochem. Sci.* **2012**, *37*, 373–380; d) E. Romero, J. R. Gomez Castellanos, G. Gadda, M. W. Fraaije, A. Mattevi, *Chem. Rev.* **2018**, *118*, 1742–1769.
[17] G. Gygli, M. F. Lucas, V. Guallar, W. J. H. van Berkel, *PLoS Comput. Biol.* **2017**, *13*, e1005787.
[18] L. Betancor, M. J. Fernandez, K. J. Weissman, P. F. Leadlay, *ChemBioChem* **2008**, *9*, 2962–2966.
[19] a) F. Fan, G. Gadda, *J. Am. Chem. Soc.* **2005**, *127*, 2067–2074; b) F. Salvi, Y. F. Wang, I. T. Weber, G. Gadda, *Acta Crystallogr. Sect. D* **2014**, *70*, 405–413; c) W. P. Dijkman, C. Binda, M. W. Fraaije, A. Mattevi, *ACS Catal.* **2015**, *5*, 1833–1839; d) W. P. Dijkman, M. W. Fraaije, *Appl. Environ. Microbiol.* **2014**, *80*, 1082–1090.
[20] a) X. Ma, B. Liang, M. Qi, H. Yun, K. Shi, Z. Li, Y. Guo, P. Yan, S. J. Liu, A. Wang, *Environ. Sci. Technol.* **2020**, *54*, 7591–7600; b) J. Zhang, W. Gan, R. Zhao, K. Yu, H. Lei, R. Li, X. Li, B. Li, *Water Res.* **2020**, *187*, 116397; c) J. Zhang, X. Li, H. Lei, R. Zhao, W. Gan, K. Zhou, B. Li, *J. Hazard. Mater.* **2022**, *426*, 128101.
[21] S. Jahandideh, L. Jaroszewski, A. Godzik, *Acta Crystallogr. Sect. D* **2014**, *70*, 627–635.
[22] J. Jumper, R. Evans, A. Pritzel, T. Green, M. Figurnov, O. Ronneberger, K. Tunyasuvunakool, R. Bates, A. Zidek, A. Potapenko, A. Bridgland, C. Meyer, S. A. A. Kohl, A. J. Ballard, A. Cowie, B. Romera-Paredes, S. Nikolov, R. Jain, J. Adler, T. Back, S. Petersen, D. Reiman, E. Clancy, M. Zielinski, M. Steinegger, M. Pacholska, T. Berghammer, S. Bodenstein, D. Silver, O. Vinyals, A. W. Senior, K. Kavukcuoglu, P. Kohli, D. Hassabis, *Nature* **2021**, *596*, 583–589.
[23] M. Kiess, H. J. Hecht, H. M. Kalisz, *Eur. J. Biochem.* **1998**, *252*, 90–99.
[24] J. P. Roth, J. P. Klinman, *Proc. Natl. Acad. Sci. USA* **2003**, *100*, 62–67.
[25] E. Krissinel, K. Henrick, *Acta Crystallogr. Sect. D* **2004**, *60*, 2256–2268.
[26] D. Liebschner, P. V. Afonine, N. W. Moriarty, B. K. Poon, O. V. Sobolev, T. C. Terwilliger, P. D. Adams, *Acta Crystallogr. Sect. D* **2017**, *73*, 148–157.
[27] a) M. Toplak, A. Matthews, R. Teufel, *Arch. Biochem. Biophys.* **2021**, *698*, 108732; b) M. Toplak, R. Teufel, *Biochemistry* **2022**, *61*, 47–56.
[28] L. K. Liu, H. Abdelwahab, J. S. Martin Del Campo, R. Mehra-Chaudhary, P. Sobrado, J. J. Tanner, *J. Biol. Chem.* **2016**, *291*, 21553–21562.
[29] F. Hollmann, I. Arends, K. Buehler, A. Schallmey, B. Buhler, *Green Chem.* **2011**, *13*, 226–265.
[30] W. V. Shaw, *CRC Crit. Rev. Biochem.* **1983**, *14*, 1–46.
[31] T. Izard, J. Ellis, *EMBO J.* **2000**, *19*, 2690–2700.
[32] a) D. Gahloth, M. S. Dunstan, D. Quaglia, E. Klumbys, M. P. Lockhart-Cairns, A. M. Hill, S. R. Derrington, N. S. Scrutton, N. J. Turner, D. Leys, *Nat. Chem. Biol.* **2017**, *13*, 975–981; b) D. Gahloth, G. A. Aleku, D. Leys, *J. Biotechnol.* **2020**, *307*, 107–113.
[33] M. Mergelsberg, M. Willistein, H. Meyer, H. J. Stark, D. F. Bechtel, A. J. Pierik, M. Boll, *Environ. Microbiol.* **2017**, *19*, 3734–3744.
[34] a) S. Kumar, G. Stecher, M. Li, C. Knyaz, K. Tamura, *Mol. Biol. Evol.* **2018**, *35*, 1547–1549; b) D. T. Jones, W. R. Taylor, J. M. Thornton, *Comput. Appl. Biosci.* **1992**, *8*, 275–282.
[35] I. Letunic, P. Bork, *Nucleic Acids Res.* **2021**, *49*, W293-W296.
[36] F. Gorrec, *J. Appl. Crystallogr.* **2009**, *42*, 1035–1042.

[37] a) W. Kabsch, *Acta Crystallogr. Sect. D* **2010**, *66*, 125–132; b) W. Kabsch, *Acta Crystallogr. Sect. D* **2010**, *66*, 133–144.
[38] P. R. Evans, G. N. Murshudov, *Acta Crystallogr. Sect. D* **2013**, *69*, 1204–1214.
[39] P. Emsley, B. Lohkamp, W. G. Scott, K. Cowtan, *Acta Crystallogr. Sect. D* **2010**, *66*, 486–501.
[40] P. D. Adams, R. W. Grosse-Kunstleve, L. W. Hung, T. R. Ioerger, A. J. McCoy, N. W. Moriarty, R. J. Read, J. C. Sacchettini, N. K. Sauter, T. C. Terwilliger, *Acta Crystallogr. Sect. D* **2002**, *58*, 1948–1954.
[41] C. J. Williams, J. J. Headd, N. W. Moriarty, M. G. Prisant, L. L. Videau, L. N. Deis, V. Verma, D. A. Keedy, B. J. Hintze, V. B. Chen, S. Jain, S. M. Lewis, W. B. Arendall 3rd, J. Snoeyink, P. D. Adams, S. C. Lovell, J. S. Richardson, D. C. Richardson, *Protein Sci.* **2018**, *27*, 293–315.

Manuscript received: November 2, 2022
Revised manuscript received: November 9, 2022
Accepted manuscript online: November 10, 2022
Version of record online: December 5, 2022